Investigation of a Lineament that Might Mark the Ground-Surface Trace of the

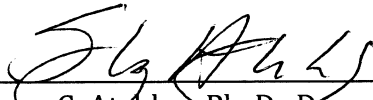Dog Valley Fault, Truckee Area, Northern California

A Thesis Submitted to the Faculty of

Baylor University

In Partial Fulfillment of the

Requirements for the Degree of

Bachelor of Science in Geology

By Jeremy A. Ashburn

Waco, Texas

July, 2015
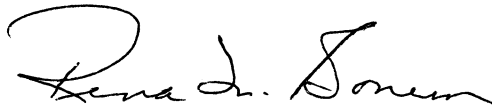
APPROVED BY THE DEPARTMENT OF GEOLOGY

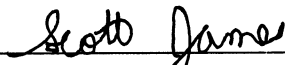Stacy C. Atchley, Ph. D., Department of Geology

APPROVED BY THE THESIS COMMITTEE

Vincent S. Cronin, Ph.D., Advisor

Rena M. Bonem, Ph.D.

Scott C. James, Ph.D.

July 13, 2015

ABSTRACT

Investigation of a Lineament that Might Mark the Ground-Surface Trace of the Dog
Valley Fault, Truckee Area, Northern California

Jeremy A. Ashburn, B.S.

Committee Chairperson: Vincent S. Cronin, Ph.D.

The magnitude-6 Truckee earthquake of 12 September 1966 has been
attributed to slip along the Dog Valley fault – a fault whose existence had not been
previously known. Two faulted outcrops in the vicinity of the Truckee earthquake
showed no evidence of slip and were not located on the same fault, and the few
observed examples of ground-surface rupture did not occur along a linear trend. As
a consequence, the trace of the Dog Valley fault is inferred but not known. Results
from SLAM analysis of smaller, more recent earthquakes from 1983 and 1992
indicated possible spatial correlation between these events and a prominent
geomorphic lineament that projects from Prosser Creek Reservoir to the Stampede
Dam. This pilot study indicates that it might be fruitful to more closely examine this
lineament in a future study that would comprehensively map the faults at the
northeast abutment of Stampede Dam, perform some modest trenching, and use
aerial LiDAR data to examine the associated geomorphology.

TABLE OF CONTENTS

Page

iv

LIST OF FIGURES

LIST OF TABLES

ACKNOWLEDGEMENTS

CHAPTER ONE

Introduction

This thesis is the third in a series of research projects conducted with the guidance

of Dr. Cronin in the northern Lake Tahoe area of northeastern California and

northwestern Nevada (fig. 1). The primary objective of these projects has been to

correlate earthquakes with seismogenic faults, which can then be used to increase seismic

safety.   Ryan Lindsay (2011) worked with all focal mechanisms that were available at

the time for earthquakes with epicenters in the northern Lake Tahoe-Truckee area.

Spatial analysis of focal mechanism solutions was used to correlate earthquakes with the

Dog Valley fault zone, the Polaris fault, West Tahoe fault, North Tahoe fault, Incline

Village fault, and a hypothesized Agate Bay fault. Tyler Reed (2013) narrowed the focus

of investigation to the Dog Valley fault zone and the Polaris fault, while also

investigating two inferred fault trends at Martis Creek and Prosser Creek.

The study area for this thesis is located in the geographic box bounded by 39.3°-

39.6° N latitude to 120.0°-120.25° W longitude, placing it between the northern Walker

Lane, the Sierra Nevada-Great Valley block, and the Northern California shear zone (fig.

1; Hammond and others, 2011). The Walker Lane is a zone of strike-slip and

extensional faulting with a dextral shear component located along the eastern edge of the

Sierra Nevada Mountains (*e.g.*, Stewart, 1988; Hammond and Thatcher, 2007; Blewitt

and others, 2009; Kreemer and others, 2009; Hammond and others, 2009, 2011; Putirka

and Busby, 2011). Displacement along Walker Lane faults serves to accommodate as

1

much as ~20-25% of the relative plate motion between the North American and Pacific plates (Hammond and others, 2011).

The current study arose from the curious fact that the ground-surface trace of the fault responsible for the largest earthquake ever recorded in the north Tahoe-Truckee area has not yet been found. The M6 Truckee earthquake occurred on 12 September 1966, and was felt from San Francisco to Salt Lake City, and from Bakersfield north to Chico, California (Kachadoorian and others, 1967). The epicenter for the *Truckee earthquake*, as it has come to be known, was located at 39.44°N latitude and 120.16°W
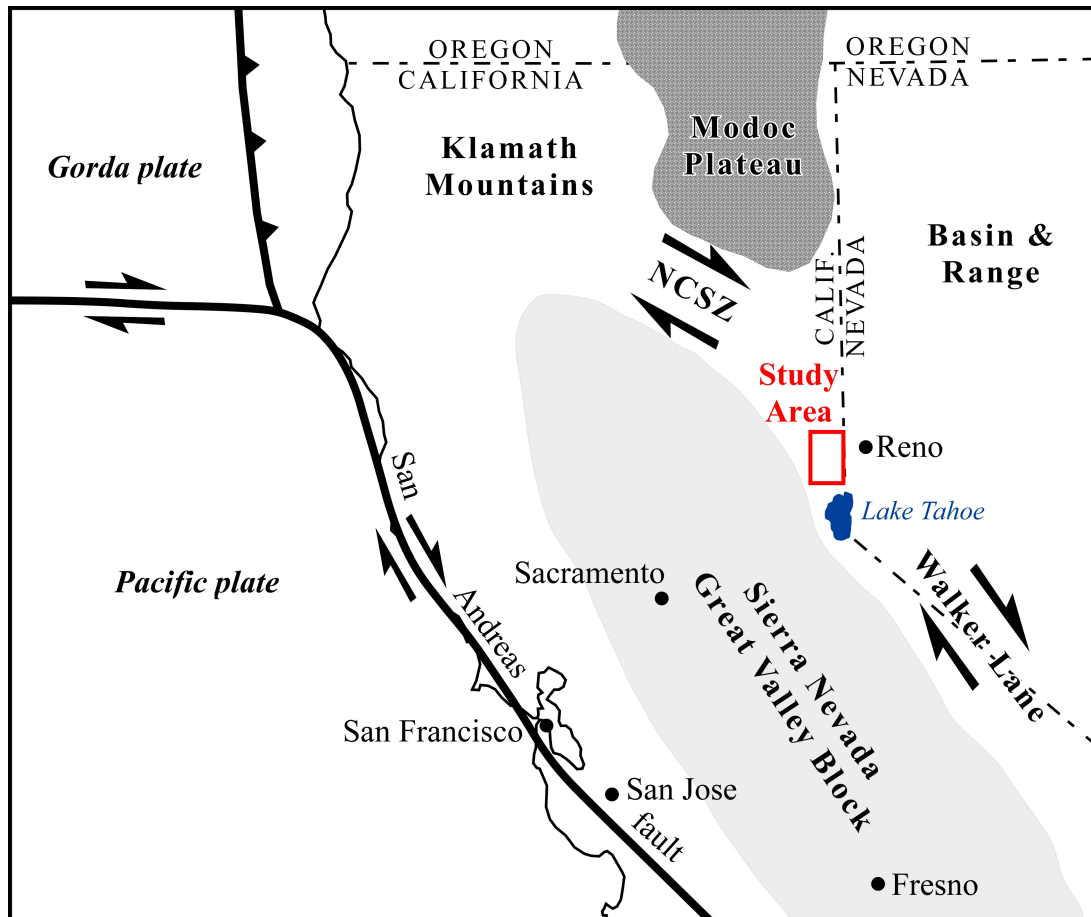
Figure 1. Location of study area (red box) within the regional tectonic context. NCSZ=Northern California Shear Zone. After Lindsay (2011).

2

longitude, approximately 13 km north-northeast of the town of Truckee, California (fig. 2; Ryall and others, 1968). The earthquake caused damage to a variety of structures, including the Prosser and Boca earth-fill dams, and generated several rock falls, landslides, and soil slumps. Field work by the U.S. Geological Survey immediately after the earthquake was able to identify several places where ground disturbances were observed in unconsolidated alluvium, but no linear rupture that might have been directly associated with a fault was found (fig. 2; Kachadoorian and others, 1967; Carter, 1966).
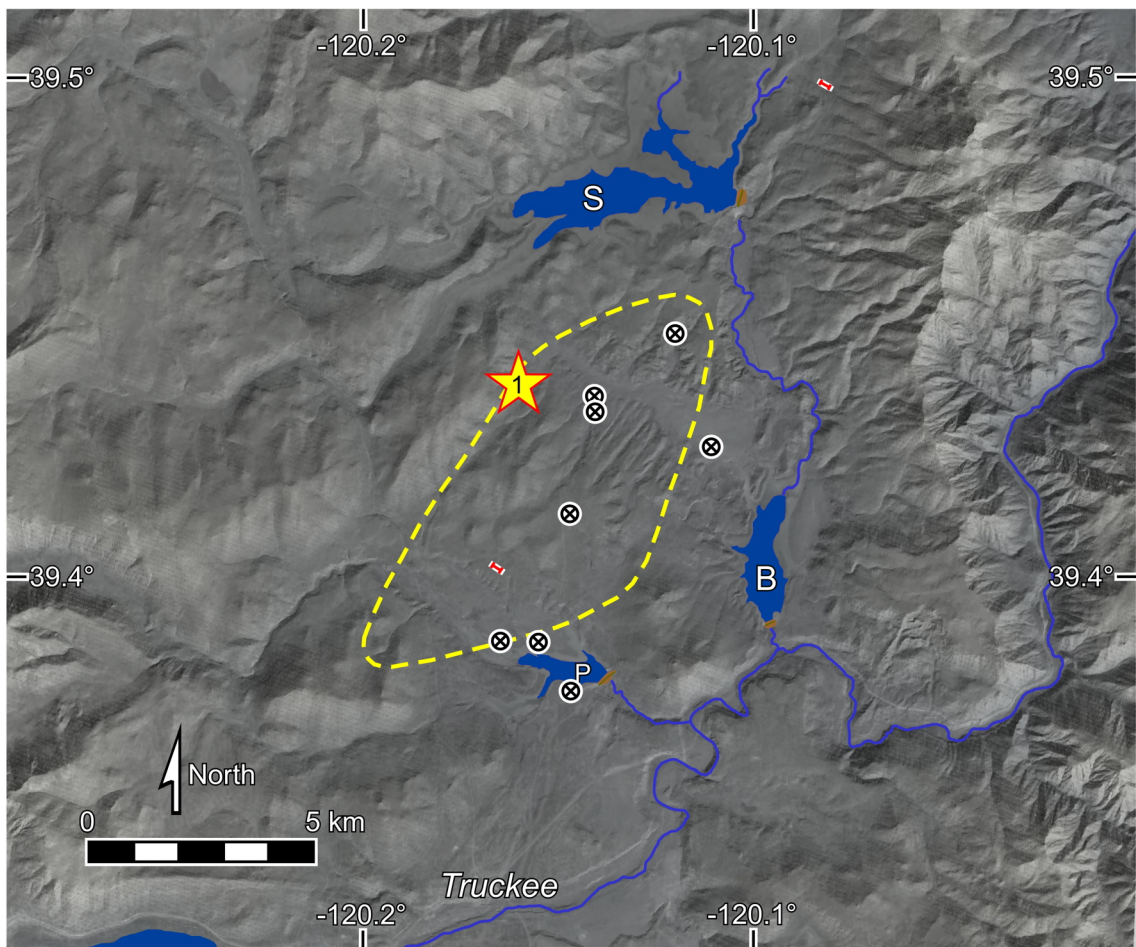
Figure 2. Epicenter of 1966 Truckee earthquake (star) and locations of ground ruptures (circles with crosses) reported by Kachadoorian and others (1967). Dashed yellow curve encloses area where most aftershocks occurred, and short red lines indicate locations of two exploratory trenches dug by the US Bureau of Reclamation (after Hawkins and others, 1986, p. 66). S=Stampede Reservoir; B=Boca Reservoir, P=Prosser Creek Reservoir.

3

Construction was in progress on the Stampede Dam at the time of the Truckee earthquake, whose epicenter was ~6 km southwest of the damsite. The cleanout excavation at the dam's base exposed several fault strands, but there is no indication from surviving records that there was displacement along any of these strands during the Truckee earthquake (Sarah Derouin of the US Bureau of Reclamation, personal communication with V.S. Cronin, 2014). Construction continued, and the dam was completed in 1970 as a 239 foot high, 1511 foot long, rolled-earth and rock-filled dam structure designed to impound 226,500 acre-feet of water in Stampede Reservoir (USBR, 2011).

The impact of a dam breach on the Truckee River has been modeled by the United States Army Corps of Engineers (Hunter and others, 2010). Modeling a breach of the Martis Creek Dam -- a structure located nearby on another tributary of the Truckee River -- indicated "the potential for large impacts to downstream areas and facilities including inundating large portions of the Reno-Sparks metropolitan area, railroads, bridges, and an Interstate Highway" (Hunter and others, 2010, 2011). As an appropriate safeguard to the devastation that could result from a dam failure, the United States Army Corps of Engineers (USACE) has maintained the elevation of the Martis Creek Reservoir at a fraction of its 20,391 acre-feet capacity (USACE, 2012). Even when compared at its full capacity, the Martis Creek Reservoir is an order of magnitude smaller than the Stampede Reservoir's capacity. When combined with the 41,110 acre-feet capacity of the Boca Reservoir directly downstream, a failure of the Stampede Dam at full capacity could send over 260,000 acre-feet of water down a vertical drop of ~440 meters along the Truckee River Gorge and through downtown Reno, destroying several towns along the way.

The U.S. Bureau of Reclamation (USBR), which operates the Stampede, Boca and Prosser Dams, sought to identify the ground-surface trace of the Dog Valley fault by performing a geomorphic analysis and trench studies. The secondary drainage network in the area from the Boca and Prosser Reservoirs to the Stampede Reservoir is characterized by unusual, linear, parallel drainages that trend northeast, broadly coincident with the trend inferred for the Dog Valley fault from interpretations of the focal mechanism and aftershock cloud of the Truckee earthquake (Greensfelder, 1968). The USBR established two paleoseismic trenches to study faulting in this area: one near Prosser Creek Reservoir and another on the southeastern side of Hoke Valley to the northeast of the Stampede Reservoir (fig. 2). Neither trench exposed a fault surface. The Hoke Valley trench exposed andesitic mudflow breccia of the Tertiary Kate Peak formation (Birkeland, 1963) that is similar to the coarse breccia exposed across the northeast abutment of Stampede Dam (Hawkins and others, 1986). The trench near Prosser Creek Reservoir was in alluvium that formed in a temporary lake formed ~1.3 Myr (Birkeland, 1963). Hawkins and others (1986, p. 75) inferred "that the lineaments are erosional forms developed on flat-lying, undeformed Prosser Creek alluvium…when the Quaternary lake that occupied the Truckee Basin was drained."

The U.S. Bureau of Reclamation conducted a geomorphic analysis along the inferred trend of the Dog Valley fault, using aerial photos taken for the USGS in 1953 and 1974, and mapped a series of subparallel geomorphic lineaments that they thought might be related to surface deformation (Hawkins and others, 1986, p. 66). The resulting map is the basis for the Dog Valley fault trace that is included in the Quaternary Fault
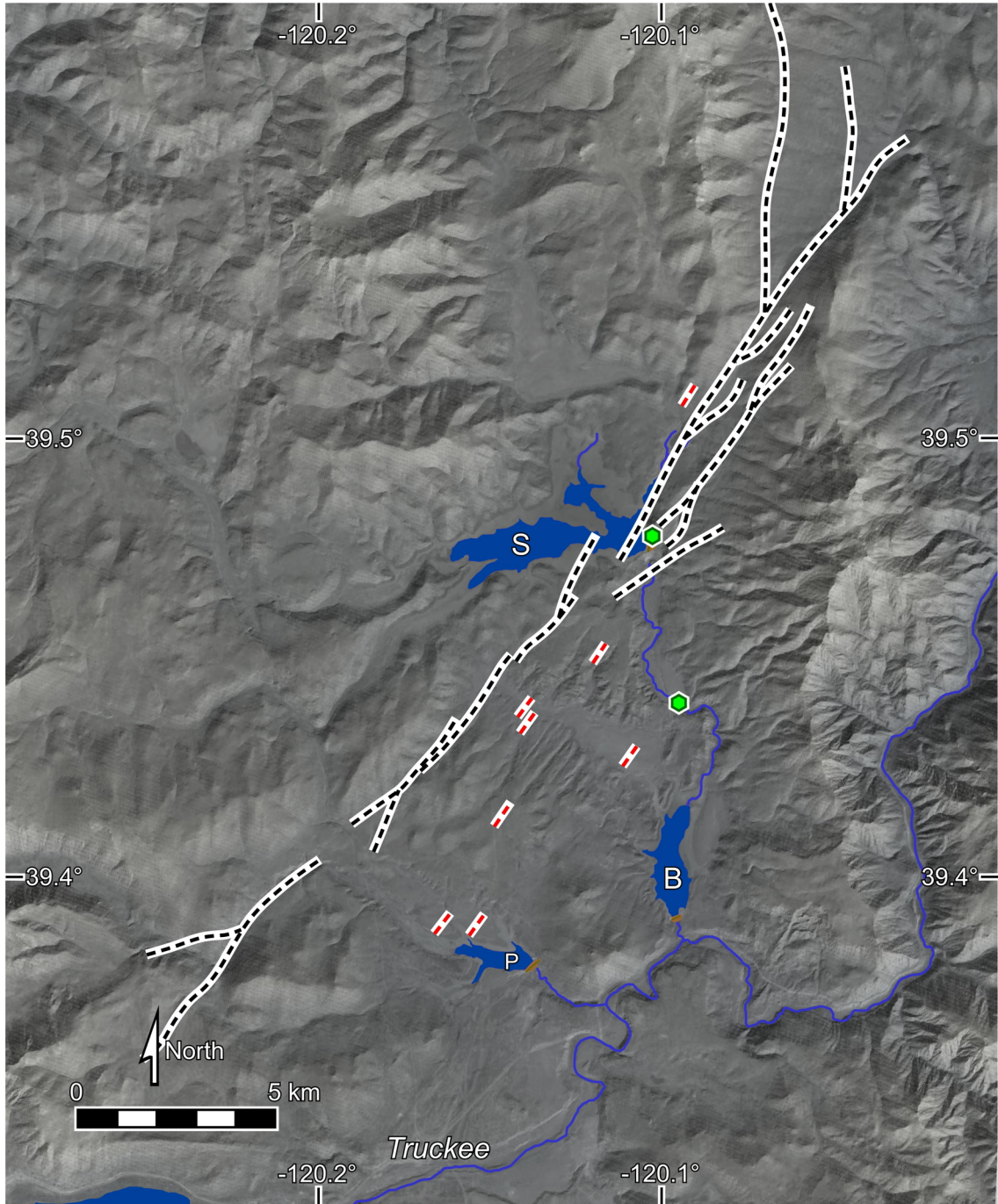
Figure 3. Trace of Dog Valley fault (black dashed curves) from the Quaternary Fault and Fold Database of the United States (USGS, 2015, after Hawkins and others, 1986, p. 66). Red dashed lines indicate locations of ground ruptures reported after the 1966 Truckee earthquake. Green hexagons are faults observed in outcrop. S=Stampede Reservoir; B=Boca Reservoir, P=Prosser Creek Reservoir.

and Fold Database of the United States (http://earthquake.usgs.gov/hazards/qfaults/; Olig

and others, 2005; Grose, 2000). This is the current understanding of the location of the

Dog Valley fault (fig. 3; *e.g.*, Olig and others, 2005).

Tyler Reed included the Truckee earthquake and the Dog Valley fault in his

Masters thesis (Reed, 2013). The uncertainty in hypocenter location was thought to be on
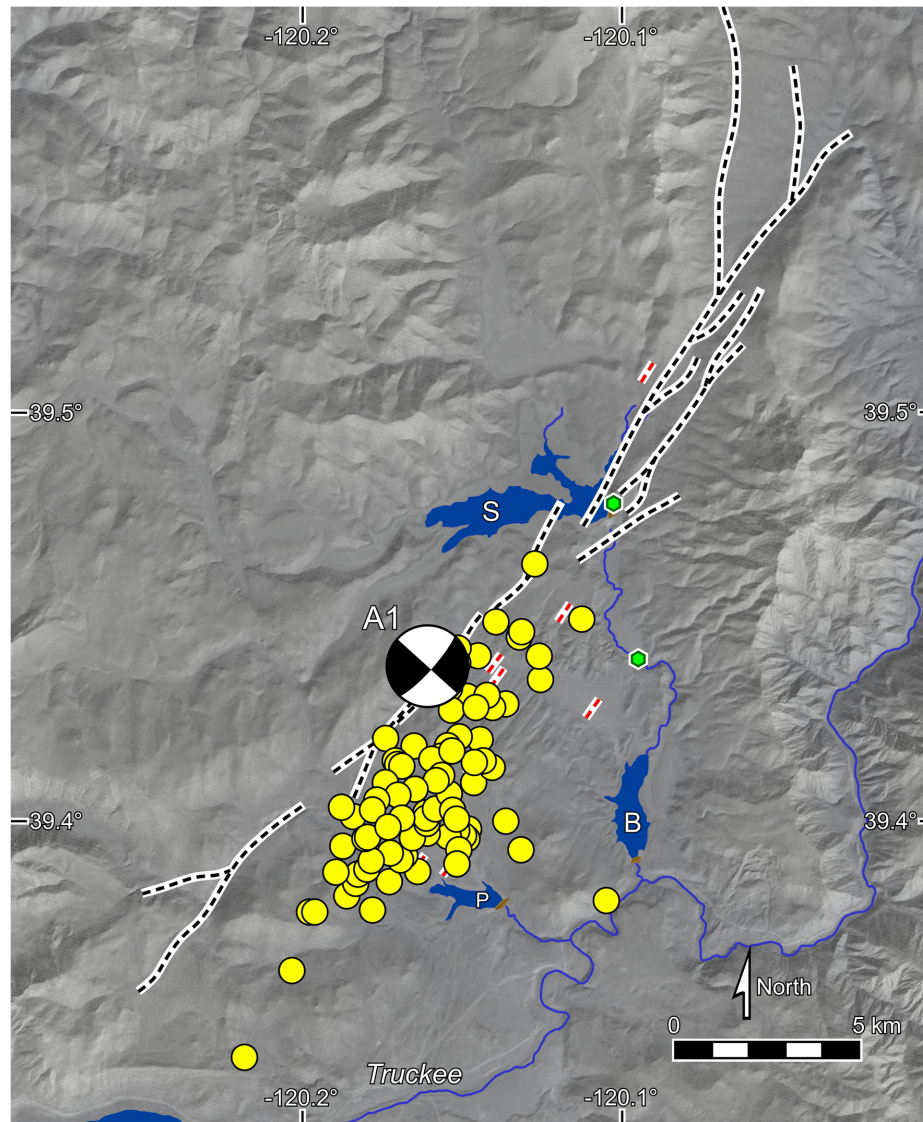
Figure 4. Focal mechanism and aftershocks (yellow circles) of 1966 Truckee earthquake (Tsai and Aki, 1970; Greensfelder, 1968). Trace of Dog Valley fault (black dashed curves) from Quaternary Fault and Fold Database of the United States (USGS, 2015). Green hexagons mark locations where faults are exposed in outcrop. S=Stampede Reservoir; B=Boca Reservoir, P=Prosser Creek Reservoir.

the order of 1-2 km (Ryall and others, 1968), and no uncertainties were given for the orientation of nodal planes in the published focal mechanisms (Ryall and others, 1968; Tsai and Aki, 1970). Reed (2013) created a map combining the focal mechanism diagram of Tsai and Aki (1970), the inferred Dog Valley fault trace from Hawkins and others (1986), the aftershock epicenters of Greensfelder (1968) and the seismo-lineament he computed using the northeast-striking nodal plane from Tsai and Aki's focal mechanism (fig. 4, from Reed's fig. 8). Given that the focal mechanism was based on a network of seismographs that was very sparse by today's standards and the aftershocks were based on a local network deployed after the Truckee earthquake, it is interesting to wonder whether the aftershock sequence might better reflect the strike of the seismogenic Dog Valley fault than the inferred traces suggested by Hawkins and others (1986).

Dr. Cronin and I reviewed the results presented in Reed's MS thesis during the spring of 2014, and noticed that the seismo-lineaments for several earthquakes overlapped with one another along the Dog Valley fault trend. Overlapping seismo-lineaments associated with similar focal mechanisms for two earthquakes might mean that both earthquakes occurred along the same fault. In the case of the Dog Valley fault, there appeared to be a few earthquakes with overlapping seismo-lineaments that might have been generated along the Dog Valley fault, and might be either distant aftershocks of the 1966 Truckee earthquake or potentially foreshocks of a future large earthquake. Within a composite seismo-lineament created using data from earthquakes recorded on 3 July 1983 and 30 August 1992, we noticed a rather strong geomorphic lineament that seemed to have a trend that coincides with the long axis of the aftershock cloud, but

8

diverged from the trend of the Dog Valley fault as inferred by Hawkins and others (1986).

Purpose

The purpose of this thesis was to investigate the relatively prominent geomorphic lineament we found by creating composite seismo-lineaments along the Dog Valley fault. I thought it possible that the actual trace of the Dog Valley fault might be along this geomorphic lineament, and not (just) along the trend inferred by Hawkins and others (1986). It is also possible that this is a zone of distributed shearing on several parallel fault strands. This is a preliminary study that might be followed by a more intensive investigation that could be undertaken as a graduate research project.

CHAPTER TWO

Methods and Primary Data

Seismo-Lineament Analysis Method

The Seismo-Lineament Analysis Method (SLAM) has been developed as a way to spatially correlate an earthquake, for which a focal mechanism has been determined, with the ground-surface trace of the fault that generated the earthquake (Cronin and others, 2008; Cronin, 2014c). SLAM involves a computer-based spatial analysis to identify the boundaries of the area within which a suspected fault plane is most likely to intersect the ground surface, a geomorphic analysis, and fieldwork to collect information about exposed faults and to evaluate hypotheses generated by the SLAM analyses.

As the compressional P wave propagates away from an earthquake hypocenter during a simple double-couple earthquake, the first motion of most particles will be either *toward* the hypocenter or *away from* the hypocenter. The particles that move toward the hypocenter are all in two quadrants on opposite sides of the hypocenter, and the other two quadrants contain all of the particles that moved away from the hypocenter. The boundaries between these four quadrants are perpendicular to each other, and are called *nodal planes*. Each focal mechanism solution specifies two nodal planes, one of which coincides with the fault that produced the earthquake and is called the *fault plane solution*. The other nodal plane is called the *auxiliary plane* (*e.g.*, Cronin, 2010; Jost and Herrmann, 1989).

A code written in *Mathematica* called *SLAMcode.nb* is used to determine the area

within which the trace of the fault that generated the earthquake is most likely to be

located if the fault is emergent at the ground surface (Cronin, 2014a). This area is called

a *seismo-lineament* (Cronin, 2014c; Cronin and others, 2008). The current version of

SLAMcode.nb uses as input a digital elevation model (DEM) of the epicentral region and

several types of data related to the earthquake: latitude and longitude of its epicenter, the

hypocenter depth (expressed in kilometers relative to sea level), and the orientation of the

nodal plane expressed as a dip direction and dip angle. Ideally, the uncertainty of each of

these parameters is available and can then be used to delineate a more reliable seismo-

lineament. Uncertainties in all of these parameters are available (or can be reasonably

inferred) for all of the earthquakes studied in this thesis, with the exception of the

unspecified uncertainties in nodal plane orientation for the 1966 Truckee earthquake

(Tsai and Aki, 1970).

The construction of the seismo-lineament can be visualized by starting with the

mean orientation of a nodal plane and the mean hypocenter (fig. 5). If no uncertainty is

specified for the hypocenter or for the nodal plane, the seismo-lineament would simply be

the curve formed by the intersection of the ground surface (defined by the DEM) and the

nodal plane as it extends upward from the hypocenter. If uncertainties in the hypocenter

depth and horizontal position are given, the uncertainty region around the hypocenter will

be either a sphere (if the vertical and horizontal uncertainties are equal) or an ellipsoid --

a biaxial ellipsoid if the horizontal uncertainty is the same in all directions and is different

from the vertical uncertainty, or a triaxial ellipsoid if the horizontal uncertainty is

elliptical. The nodal plane uncertainty volume is defined as in figure 5 for cases in which

11
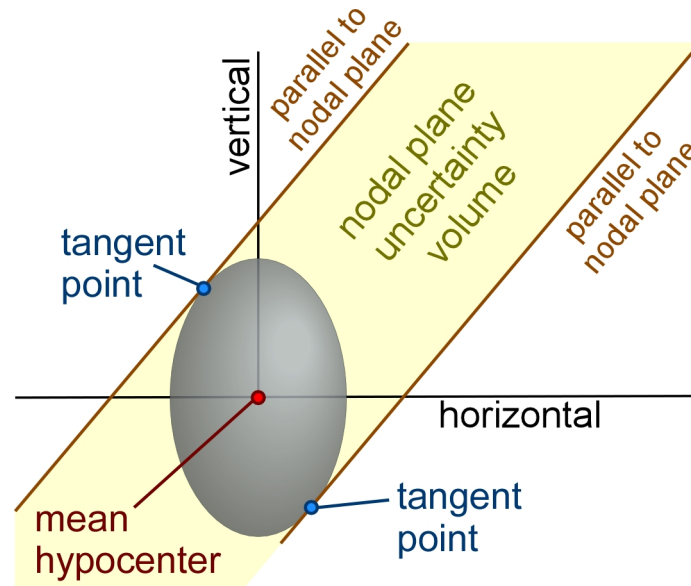
Figure 5. Cross section illustrating how the nodal plane uncertainty volume is defined in cases where the hypocenter uncertainty is known but the orientation uncertainty of the nodal plane is not known. After Lindsay (2011).

the uncertainty in nodal plane orientation is not known but the hypocenter uncertainty is known. The intersection of the nodal plane uncertainty volume with the ground surface forms the seismo-lineament.

Most of the earthquakes studied in this thesis have triaxial uncertainties in hypocenter location and orientation uncertainties reported for the nodal planes. The geometric problem of specifying the tangent points for a plane of arbitrary orientation on a triaxial ellipsoid was solved by Cronin and Cronin (2014) and incorporated in the current version of the *SLAMcode* notebook used in this thesis (Cronin, 2014a). The problem of defining the boundaries of a seismo-lineament, given a full set of uncertainties for all of the parameters, becomes a matter of defining a set of traces between the ground surface and the mean nodal plane plus-or-minus the strike uncertainty and plus-or-minus the dip-angle uncertainty when those planes are tangent to

the triaxial ellipsoid (fig. 6). The output of the *SLAMcode* notebook is a hillshade map

with the seismo-lineament boundaries (fig. 7; also see appendix figs. A1-A13).
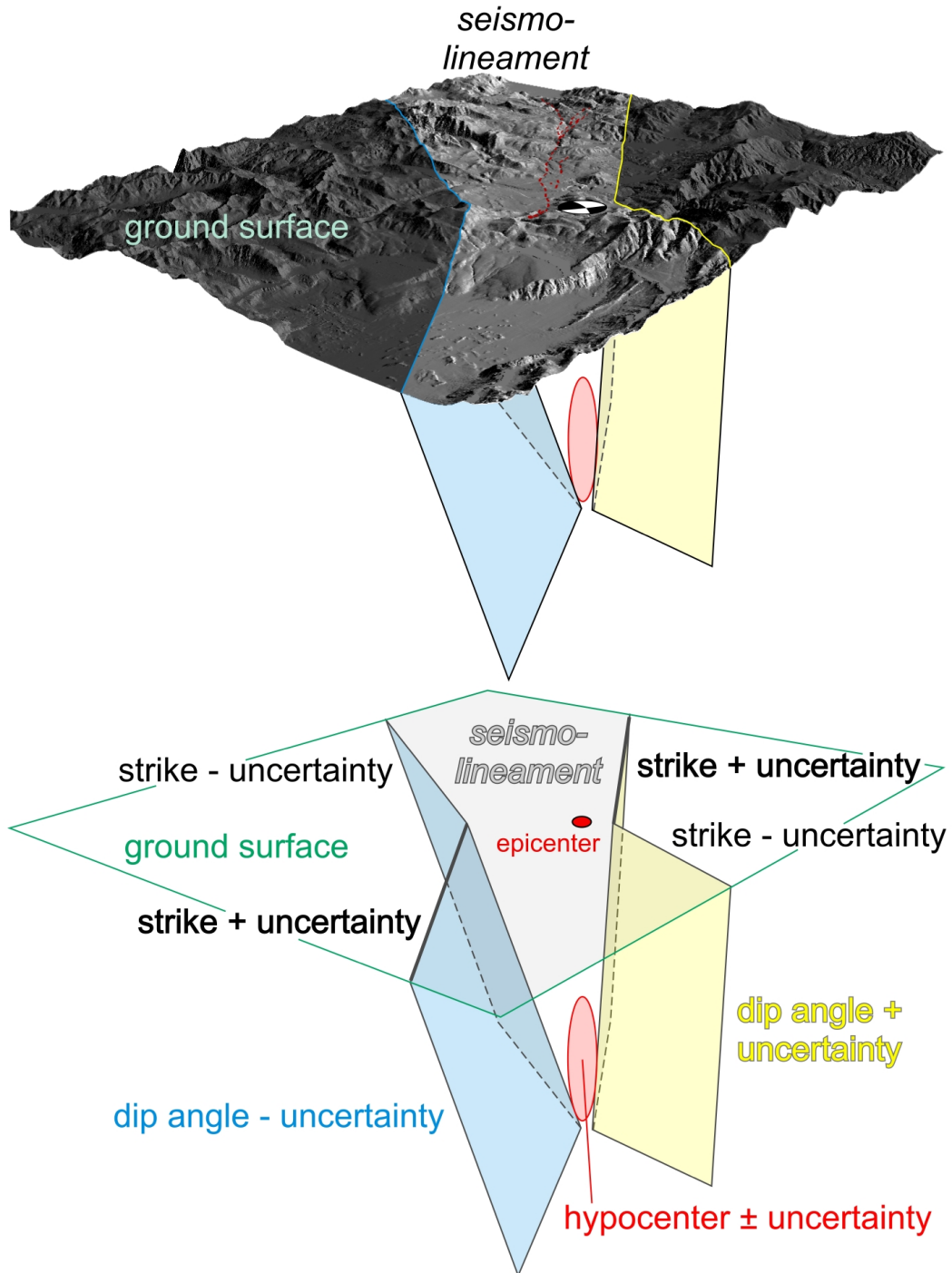
Figure 6. Top illustration shows the bow-tie-shaped seismo-lineament (light gray) for a nodal plane of the focal mechanism shown. Bottom illustration indicates the geometry of the bounding surfaces for the seismo-lineament extending from the hypocentral uncertainty ellipsoid. 2X vertical exaggeration. From Reed (2013).

13
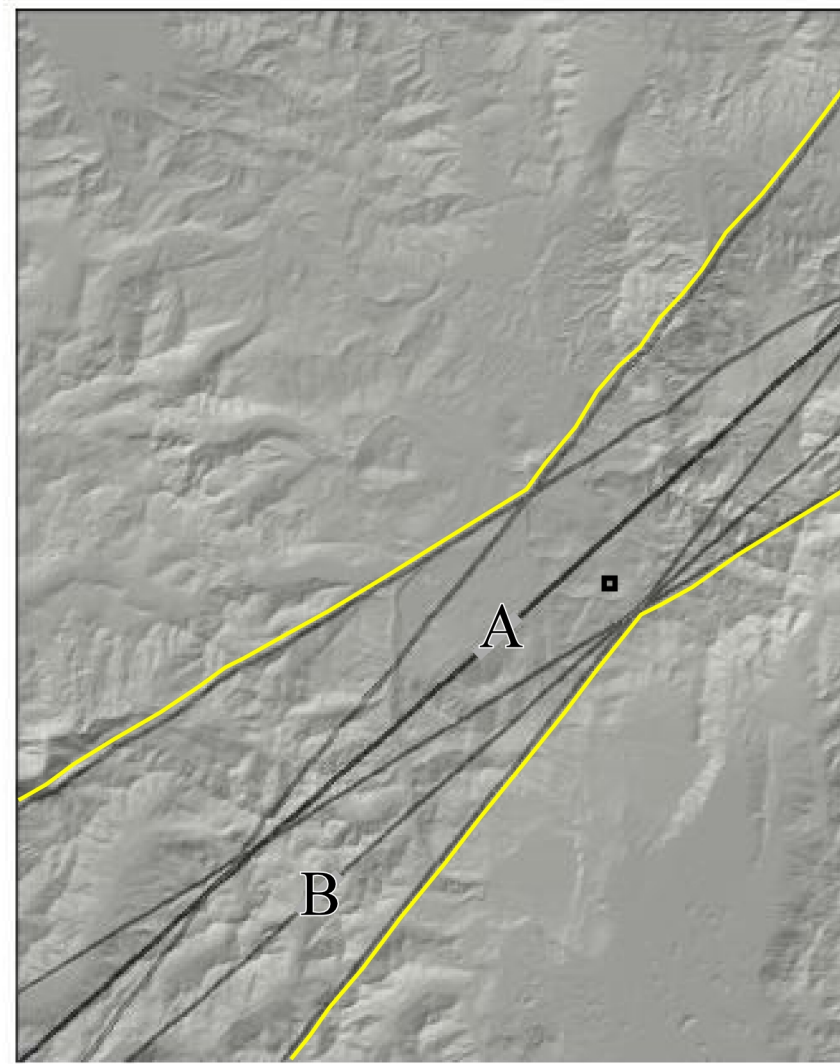
Figure 7. Annotated raw output from the SLAM code for the NE-striking nodal plane of an earthquake in the north Tahoe area. Curve A marks the ground-surface trace of the mean nodal plane. Curve B marks the trace of the nodal plane with a dip equal to the mean dip plus the dip uncertainty. Yellow curves mark the outer boundaries of all possible nodal-plane traces given the mean nodal plane orientation +/- the strike uncertainty and +/- the dip uncertainty.

SLAM employs the first-order assumptions that the earthquake data used for input are accurate, that the seismogenic fault is approximately planar, and that the fault is emergent at the ground surface. If these assumptions are valid, one can expect to locate a seismogenic fault within the uncertainty region generated by SLAM. SLAM makes use of small earthquakes that did not rupture the ground surface to find the ground-surface

trace of a seismogenic fault that, over its full history, has produced earthquakes large enough to have ruptured the surface.

Acquiring DEMs

The digital elevation model (DEM) used for the SLAM analysis was obtained from the U.S. Geological Survey National Map Viewer (USGS, 2014), initially as two ArcGrid 1/3 arc-second resolution quadrants. The two DEM files were subsequently imported into ArcGIS 10.1 to merge the files into a single seamless DEM and to convert the file to the format required by the *SLAMcode* notebook. The ArcGIS tool *Project Raster* was used to project the raster DEMs into UTM NAD1983 10N. The tool *Mosaic to New Raster* was used to combine the two quadrants into one seamless DEM. The ArcGIS tool *Raster to ASCII* was used to convert the file to ASCII. The output generated by ArcGIS is stored as a *.txt* file, which must first be converted to a *.dat* file before using it in the *SLAMcode* notebook. The file must be resaved as a *.dat* file by accessing the file properties and changing the suffix from *.txt* to *.dat*.

Two resolutions of DEM file are generally used in the SLAM process: a full-resolution file is used in geomorphic analysis, and a lower-resolution file is used by the *SLAMcode* notebook to define the boundaries of a seismo-lineament. The raw ASCII file created by combining the original ArcGrid files is cropped using the notebook *DEMdataCropper.nb*, which deletes all of the elevation data outside of the boundaries of the study area but retains full resolution within the study area. In this thesis, the DEM was cropped to the approximate boundaries of the study area: between latitudes 39.3°-39.6°N and longitudes 120.0°-120.25°W. A duplicate copy of the cropped full-resolution DEM is made, and that copy becomes input for another *Mathematica* notebook called

SLAM_data_diet.nb, which reduces the resolution of the file by a user-defined amount. The resulting lower-resolution file is a much smaller file that allows the *SLAMcode* to execute more quickly and avoids capacity problems on some computers that have less memory than needed to analyze a very large matrix. The current versions of these codes are available online at http://CroninProjects.org/Vince/SLAM/CurrentBaseCodes.html.

Earthquake Data

The primary source of earthquake data for the Tahoe-Truckee area is the Northern California Earthquake Data Center (NCEDC, http://www.ncedc.org), the Berkeley Seismological Laboratory at the University of California-Berkeley (http://seismo.berkeley.edu), and the Nevada Seismological Laboratory at the University of Nevada-Reno (http://www.unr.edu/geology/about-us/seismology). The NCEDC web site includes a search page for northern California earthquake catalogs (NCEDC, 2013; http://www.ncedc.org/ncedc/catalog-search.html). NCEDC has data on 657 earthquakes of magnitude less than 6 that occurred between 1984 and 2011 within the study area, 17 of which had magnitudes of 3.0 or greater (fig. 8). The NCEDC mechanism catalog contains focal mechanisms for 11 earthquakes with reported locations in the study area from 1968 to the present. Adding the focal mechanism published by Tsai and Aki (1970) for the 1966 Truckee earthquake, I found 12 earthquakes with focal mechanisms in the study area (table 1).

An initial location is computed for an earthquake when it occurs, based solely on the data recorded by seismographs that detected that earthquake. This is called a single-event location. Better locations can be obtained, in many cases, by considering data from

16

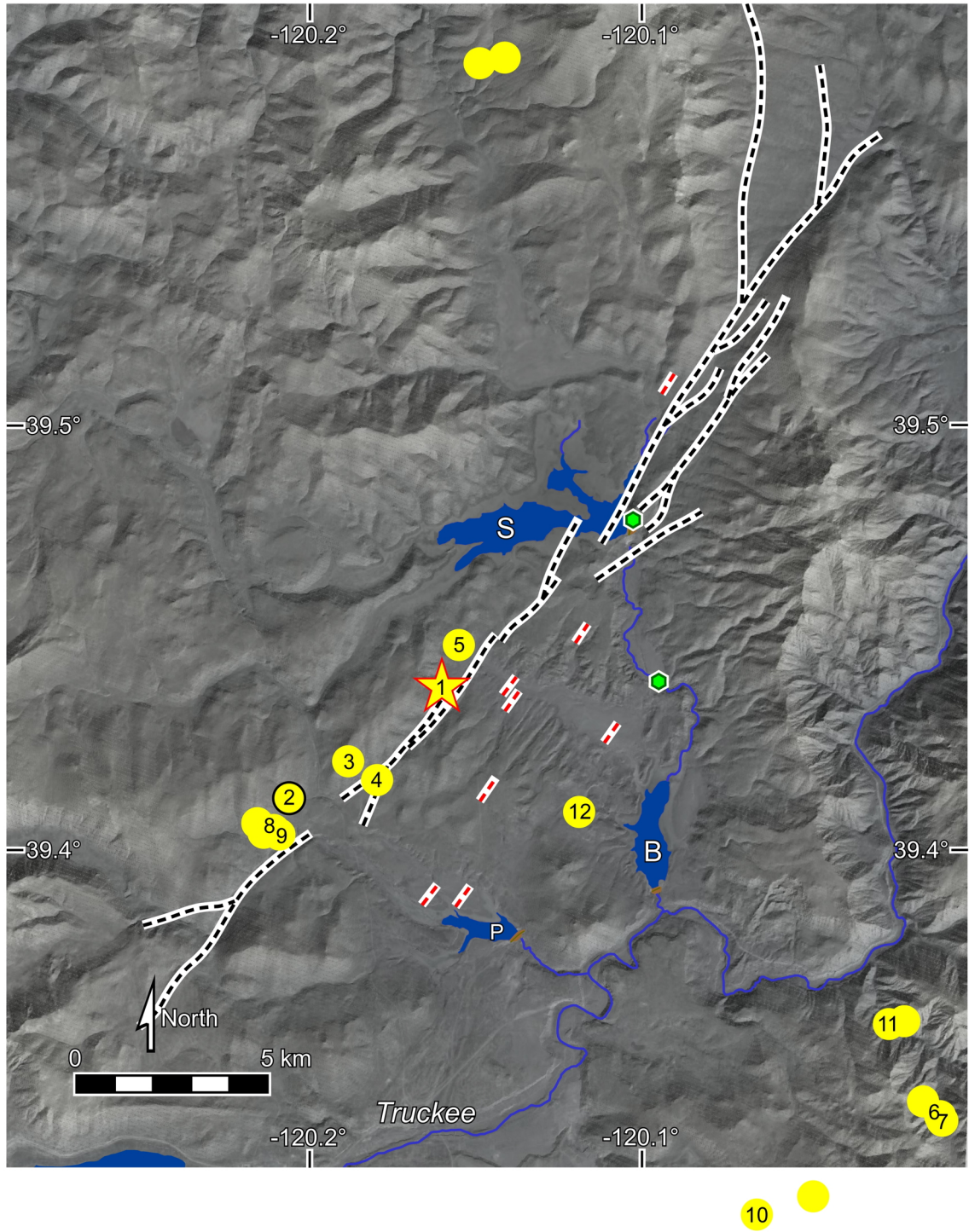Figure 8. Earthquake epicenters from NCEDC earthquake catalogs, with numbers corresponding to earthquakes listed in tables 1-3. Trace of Dog Valley fault zone (black dashed curves; USGS, 2015) with red dashed lines indicating locations of ground ruptures reported after the 1966 Truckee earthquake. Green hexagons are faults observed in outcrops. S=Stampede Reservoir; B=Boca Reservoir; P=Prosser Creek Reservoir.

Table 1. Earthquakes with published focal mechanism solutions in the study area.

Year	Month	Day	Hr	Min	Sec	Latitude °N	Longitude °W	Depth km	Mag	Mult Solns?
1966	09	12	16	41	03	39.438	120.160	10	6	yes, 2
1983	07	03	15	08	20	39.412	120.206	11.05	4	yes, 2
1992	08	30	23	42	8.447	39.42047	120.18852	5.344	3.2	yes, 2
1993	08	06	00	31	38.43	39.41621	120.18018	0.368	3.1	yes, 3
1998	01	15	15	12	14.448	39.4481	120.15511	4.636	3.8	yes, 3
2004	06	03	08	25	37.51	39.33729	120.01030	7.292	3.7	no
2004	06	03	08	54	46.35	39.33653	120.00903	7.292	3.7	no
2004	06	12	14	49	41.705	39.40479	120.21070	7.292	3.7	yes, 2
2004	06	12	15	04	18.99	39.40392	120.20964	7.352	3.4	no
2005	06	26	18	45	57.64	39.31379	120.06510	9.718	4.8	yes, 2
2010	10	18	03	44	42.63	39.35879	120.02574	4.889	3.1	yes, 2
2011	12	23	05	30	29.837	39.40871	120.11916	0.882	3	no

Data are from Waldhauser, 2013, accessed in May, 2014. Data for the M6 Truckee earthquake of 1966 are from Ryall and others (1968) and Tsai and Aki (1970).

a number of earthquakes that have occurred in the same general area, using one of a number of joint relocation strategies (*e.g.*, Jordan and Sverdrup, 1981; Waldhauser and Ellsworth, 2000; Waldhauser, 2001).

Hypocenters of the ten earthquakes listed in table 1 that occurred from 1988 through 2011 were relocated by waveform cross correlation and double-difference methods by Felix Waldhauser (2013). I downloaded Waldhauser's *Double-difference Earthquake Catalog for Northern California (1984-2011)* from http://www.ldeo.columbia.edu/~felixw/NCAeqDD/ and viewed the data in Microsoft Excel (Schaff and Waldhauser, 2005; Walhauser and Schaff, 2008; Waldhauser, 2009, 2013). A link to the README file is present on the same webpage above the download link, which provides the organizational scheme and a brief overview of the ASCII data contained in the catalog. Using Excel's sorting function to sort the data by latitude, I isolated and extracted the data for earthquakes reported in the study area (*i.e.*, latitude

39.3°-39.6°N and longitude 120.0°-120.25°W). Obtaining these data directly from the site hosted by Waldhauser at the Lamont Doherty Earth Observatory provides access to the triaxial hypocentral uncertainty data that are lacking in the double-difference catalog accessible online through the NCEDC search page. The hypocenter for the 3 July 1983 event, which predates the events in Waldhauser's catalog, was obtained through the NCEDC search page from the USGS NCSN single-event catalog, and the hypocenter for the 1966 Truckee earthquake was determined by Ryall and others (1968). These data are presented in table 2.

I noticed that earthquakes A6, A7, A10 and A11 all have relocated epicenters that are more than 14 km southeast of the inferred trace of the Dog Valley fault (fig. 8). Tyler Reed did not correlate any of these earthquakes with the Dog Valley fault in his MS thesis (Reed, 2013). The preferred fault plane solution for the 1966 Truckee earthquake is a pure left-lateral fault oriented 44, 80SE (Tsai and Aki, 1970), so epicenters of earthquakes associated with the Dog Valley fault would be expected to be located near the fault trace. The focal mechanisms for A6, A7 and A11 were normal-oblique, and the focal mechanisms for A10 were either pure normal or left-reverse-oblique on a steep plane that would be parallel to the inferred trace of the Dog Valley fault but offset more than 10 km to the southeast. For these reasons, I excluded earthquakes A6, A7, A10 and A11 from further consideration even though their epicenters were located within the rectangular boundaries of the study area.

All but one of the focal mechanisms used in this study are from the NCEDC *Mechanism Catalog (1968-Present)*, accessed via the NCEDC search page (table 3). The

Table 2. Location and magnitude data for earthquakes used in this thesis.

Earthquake Number	Date ID yyyyMMddhhmm	Latitude °N	Longitude °W	Depth km	Major Horiz Uncert (km)	Minor Horiz Uncert (km)	Azimuth of Major Horiz Uncert	Vertical Uncert (km)	Magnitude
A1	196609121641	39.438	120.160	10	2	2	45°	2	6
A2	198307031508	39.412	120.206	11.05	0.3	0.3	45°	0.8	4
A3	199208302342	39.42047	120.18852	5.344	0.539	0.026	64°	0.154	3.2
A4	199308060031	39.41621	120.18018	0.368	0.474	0.023	64°	2.394	3.1
A5	199801151512	39.4481	120.15511	4.636	0.43	0.028	64°	0.167	3.8
A6	200406030825	39.33729	120.01030	6.620	0.030	0.010	100°	0.040	3.0
A7	200406030854	39.33653	120.00903	6.874	0.031	0.021	80°	0.044	4.2
A8	200406121449	39.40479	120.21070	7.292	0.032	0.021	74°	0.057	3.7
A9	200406121504	39.40392	120.20964	7.350	0.035	0.019	64°	0.053	3.4
A10	200506261845	39.31379	120.06510	9.718	0.069	0.047	93°	0.092	4.8
A11	201010180344	39.35879	120.02574	4.889	0.049	0.025	45°	0.212	3.1
A12	201112230530	39.40871	120.11916	0.882	0.026	0.020	82°	0.172	3

Data are from Waldhauser (2013), accessed online at http://www.ldeo.columbia.edu/~felixw/NCAeqDD/ in May, 2014. Data for M6 Truckee earthquake of 1966 are from Ryall and others (1968) and Tsai and Aki (1970). Data for 3 July 1983 event are from the regular NCEDC catalog.

data were queried by the area of interest and output in Fpfit format (Reasenberg and

Oppenheimer, 1985; the Fpfit output format is explained at http://www.ncedc.org/ftp/

pub/doc/cat5/ncsn.mech.txt). The focal mechanism from the 1966 Truckee earthquake is

from Tsai and Aki (1970). The focal mechanism diagrams were produced using the

Mathematica Computable Document Format file *Earthquake Focal Mechanism*

(Scherbaum and others, 2009), operating on data from table 3. The right-hand-rule strike

for each nodal plane is found by subtracting 90° from each dip direction listed.

pub/doc/cat5/ncsn.mech.txt).

Table 3. Focal mechanisms for earthquakes near the Dog Valley fault.

Earthquake Number	NE/SW-Striking Nodal Plane			Strike Uncert (°)	Dip Uncert (°)	Rake Uncert (°)
	Dip Direction	Dip Angle	Rake			
A1	134	80	180	--	--	--
A2-A	300	80	20	8	13	30
A3-A	301	61	12	15	25	25
A4-A	333	48	59	18	13	40
A4-B	115	50	-70	13	3	5
A4-C	325	90	30	23	28	10
A5-A	331	41	49	20	8	55
A5-C	290	35	30	10	23	10
A5-C	175	73	121	10	23	10
A8-A	145	75	-20	8	40	35
A8-B	319	63	-53	8	10	15
A9	335	85	40	10	18	20
A12	145	80	0	10	33	30

Data are from the Northern California Earthquake Data Center Mechanism Catalog, accessed online at
http://www.ncedc.org/ncedc/catalog-search.html in May, 2014. Data for M6 Truckee earthquake
are from Ryall and others (1968) and Tsai and Aki (1970).

Geomorphic Analysis

The geomorphic analysis of the DEM was performed by directly viewing the map in two dimensions and by displaying it in three dimensions in ArcGIS 10.1 *ArcScene.* In both cases, the DEM was illuminated at a low angle in a direction perpendicular to the azimuth of the nodal plane strike used to construct the uncertainty swath. This served to accentuate any topographic features that may be aligned with the seismo-lineament by illuminating slopes that have an aspect parallel to the lineament. In addition, variable degrees of vertical exaggeration were applied in *ArcScene* to further expose any topographic features that may be coincident with a suspected fault.

Fault displacement at the ground surface can lead to the development of several different geomorphic features that can be used to locate the causative fault. A list of some of those features was provided in Cronin and others (2008) and reproduced here as table 4.

The purpose of this thesis was to investigate one particular geomorphic lineament that was noticed in a composite seismo-lineament made using data from earthquakes A2 and A3 (Ashburn and others, 2014). That lineament extended from the vicinity of Prosser Creek Reservoir to Stampede Dam, and is best viewed using a hillshade map based on a DEM, with illumination from ~121-138° and 301-318° at a low elevation. I used the higher-resolution cropped DEM, with a cell spacing of ~9 m, and made JPEG images of the corresponding hillshade images using the *Mathematica* notebook *MakeLitHillshade.nb*, which is accessible online via http://croninprojects.org/Vince/ SLAM/CurrentBaseCodes.html (fig. 9).
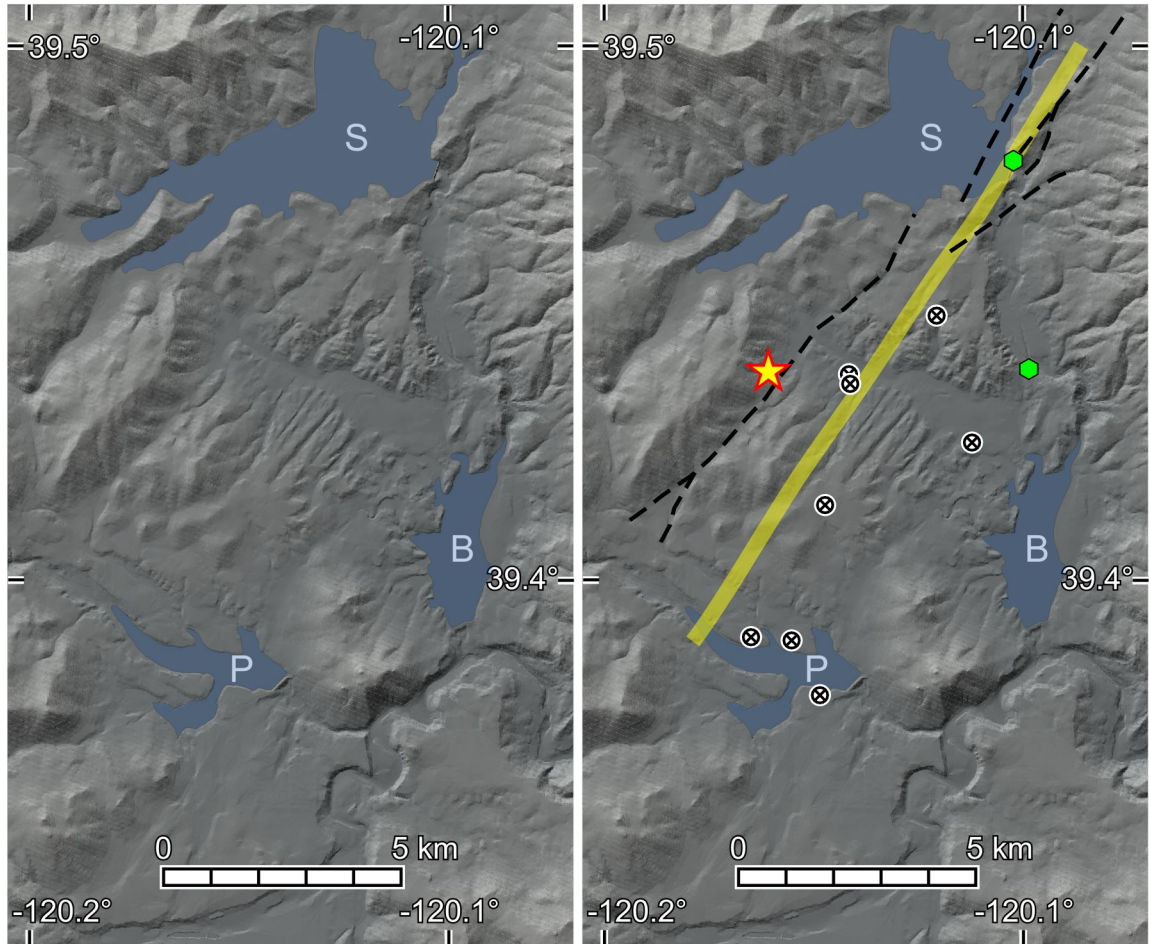
Figure 9. Hillshade images illumined at low angle from azimuths 121° and 138°, combined by transparency. Yellow curve on the right image indicates the geomorphic lineament that I studied in this thesis. Black dashed curves are the inferred trace of the Dog Valley fault (USGS, 2015). Yellow star is the epicenter of the 1966 Truckee earthquake. Circles with black crosses mark places where "broken ground" was mapped after the Truckee earthquake (Kachadoorian and others, 1967). Green hexagons are faults observed in outcrops. S=Stampede Reservoir; B=Boca Reservoir; P=Prosser Creek Reservoir.

Table 4. Geomorphic indicators of faulting

Stream channels that are aligned on opposite sides of a drainage divide

Lower-order (smaller) stream channel aligned across a higher-order stream channel

An anomalously straight segment of a stream channel

Aligned straight segments of one or more stream channels

Lower-order stream channel whose trend is directed upstream relative to the higher-order stream it intersects, so that water flowing from the smaller stream into the larger stream must change directions through an obtuse angle

Abrupt changes in gradient along a stream channel

A stream channel that steps down in the direction of flow, indicated by rapids or a waterfall (knickpoint)

A stream channel that steps up in the direction of flow, indicated by a pond

Apparent lateral deflection of an incised stream channel or floodplain

Abrupt changes in gradient along a ridge crest

A ridge crest that steps down abruptly in the direction of decreasing elevation

A ridge crest that steps up in the direction of decreasing elevation

A saddle in the ridge crest

Apparent lateral deflection of a ridge crest

Abrupt changes in the gradient of a surface localized along a narrow linear step (fault scarp)

Benches or faceted spurs at the base of ridges that are apparently unrelated to coastal or fluvial erosion

A set of ridges in an en echelon array

A topographic basin along a linear trough (pull-apart basin, sag pond)

A topographic hill along a linear trough (pop-up, pressure ridge)

A ridge across the mouth of a stream drainage that is not a glacial moraine (shutter ridge)

From Cronin and others, 2008, after Ray, 1960; Miller, 1961; Wesson and others, 1975; Bonilla, 1982; Cronin and others, 1993; McCalpin, 2009; and Burbank and Anderson, 2001

Fieldwork

Field observations were made primarily in exposures around Stampede Dam and

Reservoir, along the Little Truckee River downstream of Stampede Dam, and at several

locations where a public road intersects the geomorphic lineament that is of interest in

this thesis (fig. 9). A total of four days were spent conducting fieldwork in this area.

While the northeast and southwest section of the lineament fell within National Forest

public access land surrounding Stampede and Prosser Creek Reservoirs, the majority of

24

the central lineament was on private land, which reduced access to sites along this section lineament to those that could be accessed and observed solely from public roads.

The main objective of the field study was to locate any faults exposed in outcrop along the geomorphic lineament and to obtain strike and dip data that can be used to evaluate whether that fault spatially correlates with a fault-plane solution. We sought to collect several types of information when a fault was located, including the lithology on both sides of the fault, the presence of shear striae and their respective orientations, the approximate width of the fault core, the GPS coordinates of the fault, and the orientation of the fault surface. Exposed faults were excavated using rock hammers, garden trowels, and putty knives so that strike and dip measurements could be made directly from the sidewall of the fault. If it was not feasible to excavate the fault enough to directly place the Brunton compass on fault wall, a field notebook was held in place parallel to the fault wall and measurements were taken from the surface of the field notebook.

A minimum of seven strike-and-dip measurements were obtained from each fault that could produce them for the purpose of determining an average orientation with appropriate uncertainties for each fault. Site mean orientations and associated uncertainties were computed using Fisher statistics (Fisher, 1953; Cronin, 2008, 2014b). The average fault orientation data with their respective uncertainties could then by compared to the orientation of the nodal plane generated by SLAM to examine whether or not the faults could be correlated.

We only found one area that had accessible exposed faults along the geomorphic lineament we investigated, due to the thick glacial sediments and forests that cover most of the field area. That area was along the northeast abutment of Stampede Dam, both

25

along the road that crosses the top of the dam and along the exposed shoreface on the reservoir-side of the dam. Severe drought conditions have resulted in drastic lowering of the lake level in all of the reservoirs in the study area, exposing the shoreface that would normally be under water. In order to assess the remaining length of the lineament, a search for surface features that may be related to faulting was performed along all accessible roadways that intersected the lineament with the aid of aerial imagery obtained from Google Earth. These features include linear boundaries in vegetation, linear drainage channels parallel to the nodal plane, and elongate meadows parallel to the nodal plane (Cronin and others, 2008). When the orientation of identified features suggested that they were aligned with the lineament, they were photographed in both directions along the lineament, and the location of the site was determined using a commercial hand-held GPS receiver with a nominal resolution of several meters.

CHAPTER THREE

Results

Seismo-Lineament Analysis

The main objective of the seismo-lineament analysis in this thesis study is to

determine which of the seven earthquakes other than the Truckee earthquake (A1) listed

in table 3 can be spatially correlated with the Dog Valley fault, as its trace is currently

understood (USGS, 2015). Current understanding of the Dog Valley fault is largely

dependent on the hypocenter location and focal mechanism of the Truckee earthquake

(Ryall and others, 1968; Tsai and Aki, 1970) and the hypocenters of the subsequent

aftershocks (Greensfelder, 1968; Hawkins and others, 1986). Of the seven earthquakes

analyzed using SLAM, three have seismo-lineaments that overlap with the general trend

of the Dog Valley fault and have focal mechanisms that are similar to the Truckee

earthquake: A2, A3, and A8.

A1: Truckee earthquake, 12 September 1966

The seismo-lineament derived using the hypocenter determined by Ryall and others

(1968) and the focal mechanism of Tsai and Aki (1970) forms a linear swath across the

map, extending from the middle of Stampede Reservoir to west of Donner Lake to the

southwest (fig. 10). Neither paper specified the corresponding uncertainties. Following

Reed (2013), we made reasonable assumptions about the horizontal and vertical

uncertainties in hypocenter location, based on comments in Ryall and others (1968) that

the depth uncertainty might be on the order of 1-2 km. Reed (2013) and I assumed

vertical and horizontal uncertainties of 2 km in the *SLAMcode* run for the Truckee

earthquake. Data from only eight permanent seismograph stations were used to locate the

main Truckee earthquake, while the location of aftershock hypocenters was aided by a network of portable seismographs. Hence, the aftershocks are likely to be better located than the main Truckee earthquake.
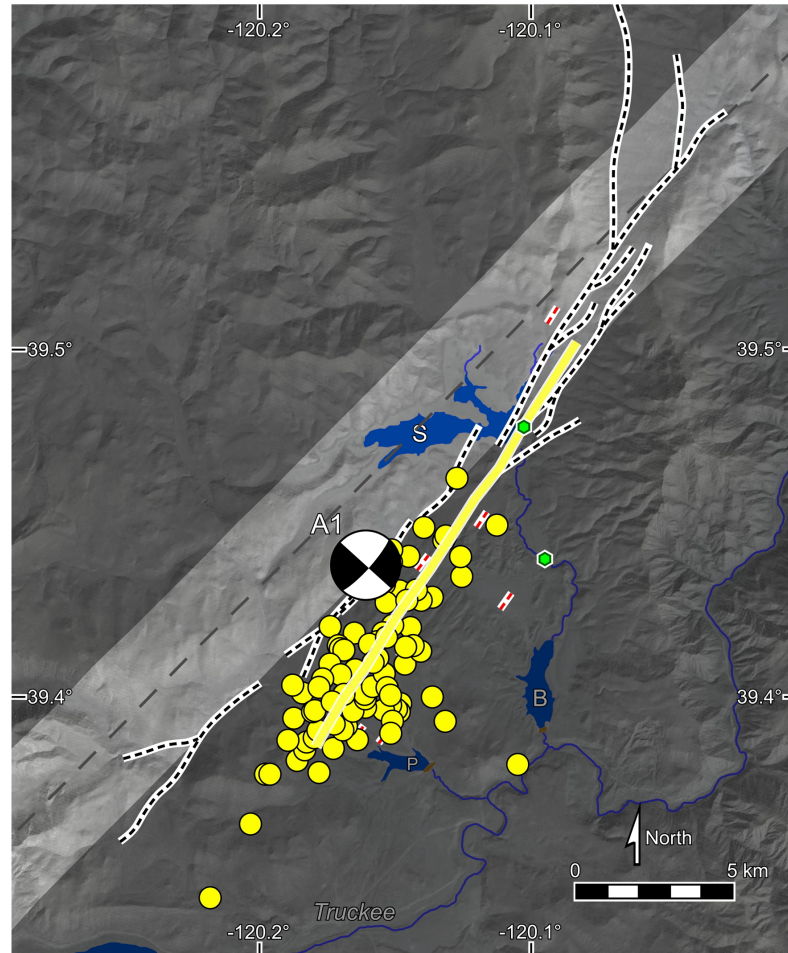

Figure 10. Map of NE-trending seismo-lineament (light gray) of the M 6.0 Truckee earthquake of 12 September 1966. Epicenter marked by focal mechanism diagram (Tsai and Aki, 1970). Yellow circles mark aftershock epicenters (Greensfelder, 1968). Yellow curve is the geomorphic lineament investigated in this research. Black dashed curve is inferred trace of Dog Valley fault (USGS, 2015). Green hexagons mark faults exposed in outcrops.

A2: M 4 earthquake, 3 July 1983

The seismo-lineament determined for the M 4.0 earthquake of 3 July 1983 earthquake overlapped the inferred trace of the Dog Valley fault and the area containing the epicenters of the 1966 earthquake aftershocks (fig 11). The strike of the northeast-

trending nodal plane for event A2 is nearly parallel with the geomorphic lineament that I investigated, which is located in the middle of this seismo-lineament.

A3: M 3.2 earthquake, 30 August 1992

The seismo-lineament determined for the M 3.2 earthquake of 30 August 1992 provided the best fit for the 1966 earthquake aftershocks out of all of the earthquakes analyzed (fig. 12). The uncertainty swath generated from this earthquake still enclosed the majority of the inferred Dog Valley fault. The strike of the northeast-trending nodal plane for event A3 is nearly parallel with that of event A2 as well as with the geomorphic lineament that I investigated, which is located in the middle of this seismo-lineament.

A8: M 3.7 earthquake, 12 June 2004

Two focal mechanisms were reported in the NCEDC mechanism catalog for the M 3.7 earthquake that occurred at 14 hours 49 minutes on 12 June 2004 (event A8). A second earthquake occurred 15 minutes later (event A9), within about a kilometer of the same location but with a different left-oblique focal mechanism that is incompatible with the Dog Valley fault. Both of these earthquakes occurred at or near the junction of the Dog Valley fault and the Polaris fault (Reed, 2013; Hunter and others, 2011).   The NE-striking nodal plane for focal mechanism A of event A8 has a dip uncertainty of 40° (table 3), so the resulting seismo-lineament is quite wide and encompasses the Dog Valley fault and the geomorphic lineament I investigated (fig. 13). The dip-angle uncertainty for focal mechanism B is 10°, so the seismo-lineament is much narrower and does not overlap the Dog Valley fault or most of the geomorphic lineament.

Figure 11. Hillshade image of the NE-trending seismo-lineament (lighter gray) of the M 4.0 earthquake of 3 July 1983. The epicenter of event A2 is marked by its focal mechanism diagram. Inferred location of the Dog Valley fault is marked by dashed black curves. Red dashed lines mark places where "broken ground" was observed after the Truckee earthquake, whose epicenter is marked by the star. Yellow curve is the geomorphic lineament investigated in this research.
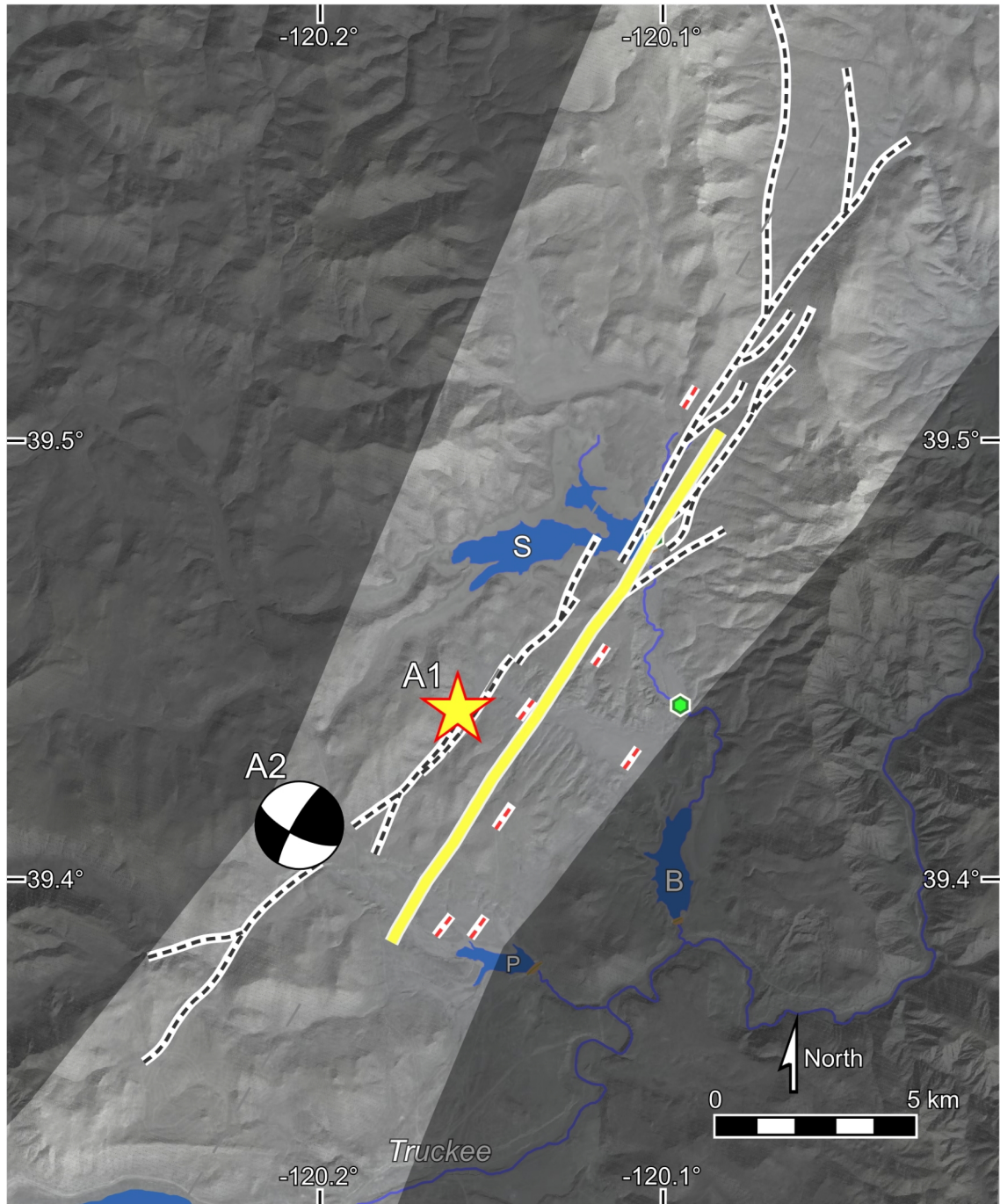
Figure 12. Hillshade image of the NE-trending seismo-lineament (light gray) of the M 3.2 earthquake of 30 August 1992. The epicenter of event A3 is marked by its focal mechanism diagram. Inferred location of the Dog Valley fault is marked by dashed black curves. Red dashed lines mark places where "broken ground" was observed after the Truckee earthquake, whose epicenter is marked by the star. Yellow curve is the geomorphic lineament investigated in this research.
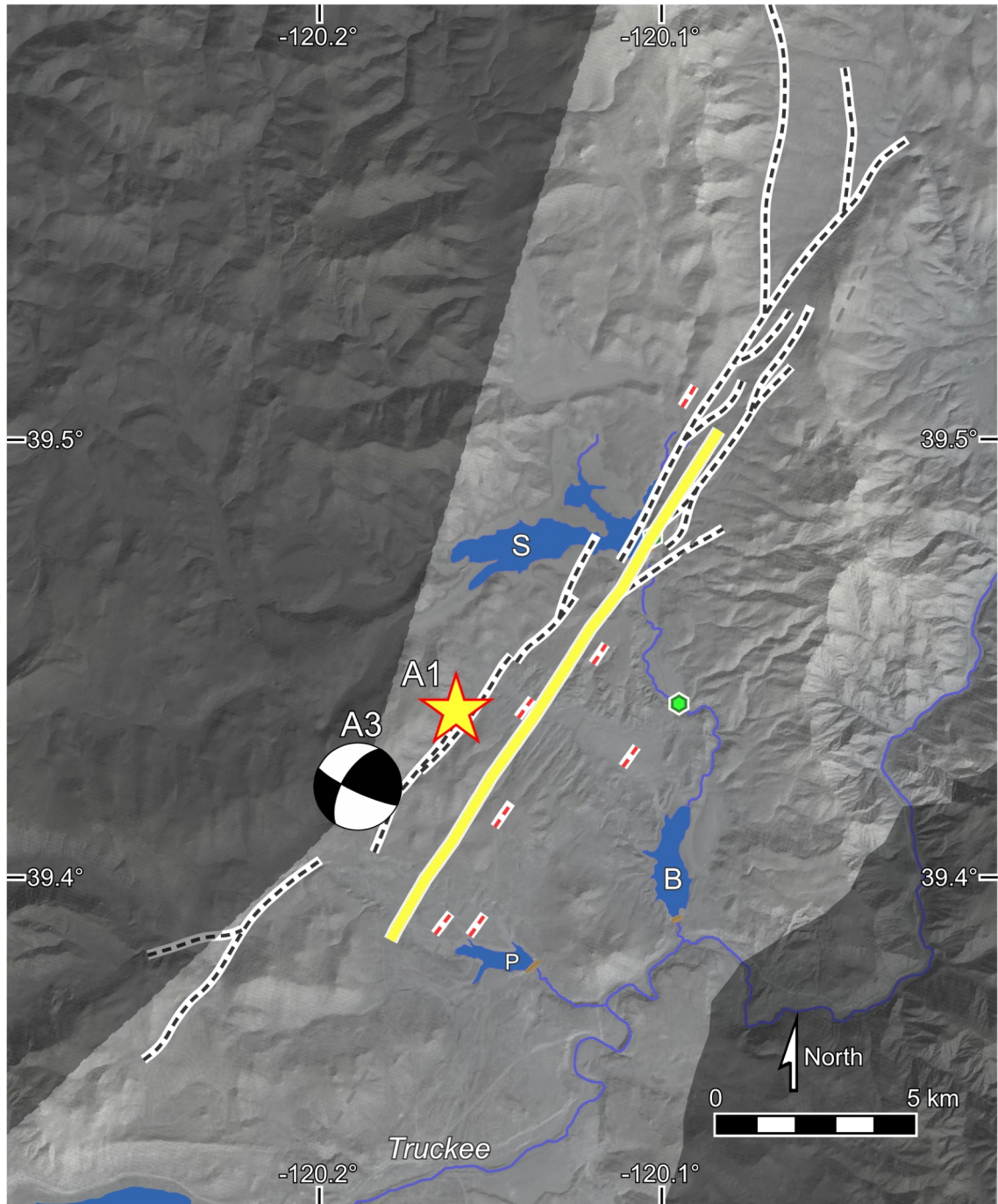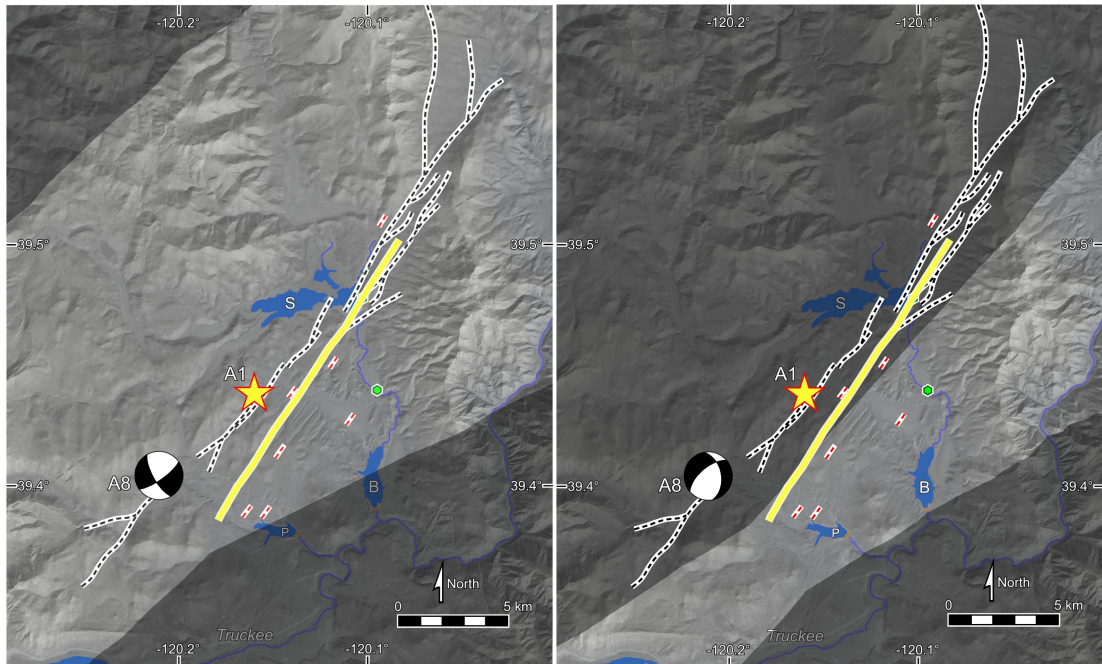
Figure 13. Hillshade images of the NE-trending seismo-lineaments (lighter gray) of the two focal mechanisms determined for the M 3.7 earthquake of 12 June 2004. Focal mechanism A8A is shown on the left map, and focal mechanism A8B is on the right map. Inferred location of the Dog Valley fault is marked by dashed black curves. Red dashed lines mark places where "broken ground" was observed after the Truckee earthquake (Kachadoorian and others, 1967), whose epicenter is marked by the star. Yellow curve is the geomorphic lineament investigated in this research.

The epicenters of events A1, A2, A3 and A8 plot along a linear trend that is parallel to the inferred trace of the Dog Valley fault as well as with the geomorphic lineament I investigated (fig. 14). Combining the seismo-lineaments of events A2, A3 and A4 provides an interesting roadmap for where to look for the ground-surface trace of a single seismogenic fault that might have produced these earthquakes. The geomorphic lineament that I investigated is parallel to and mid-way between the traces of the mean NE-striking nodal planes for events A2 and A3, assuming that both of these nodal planes pass through their respective mean hypocenter locations. This trend also agrees well with the long axis of the aftershock cloud (figure 14).

32

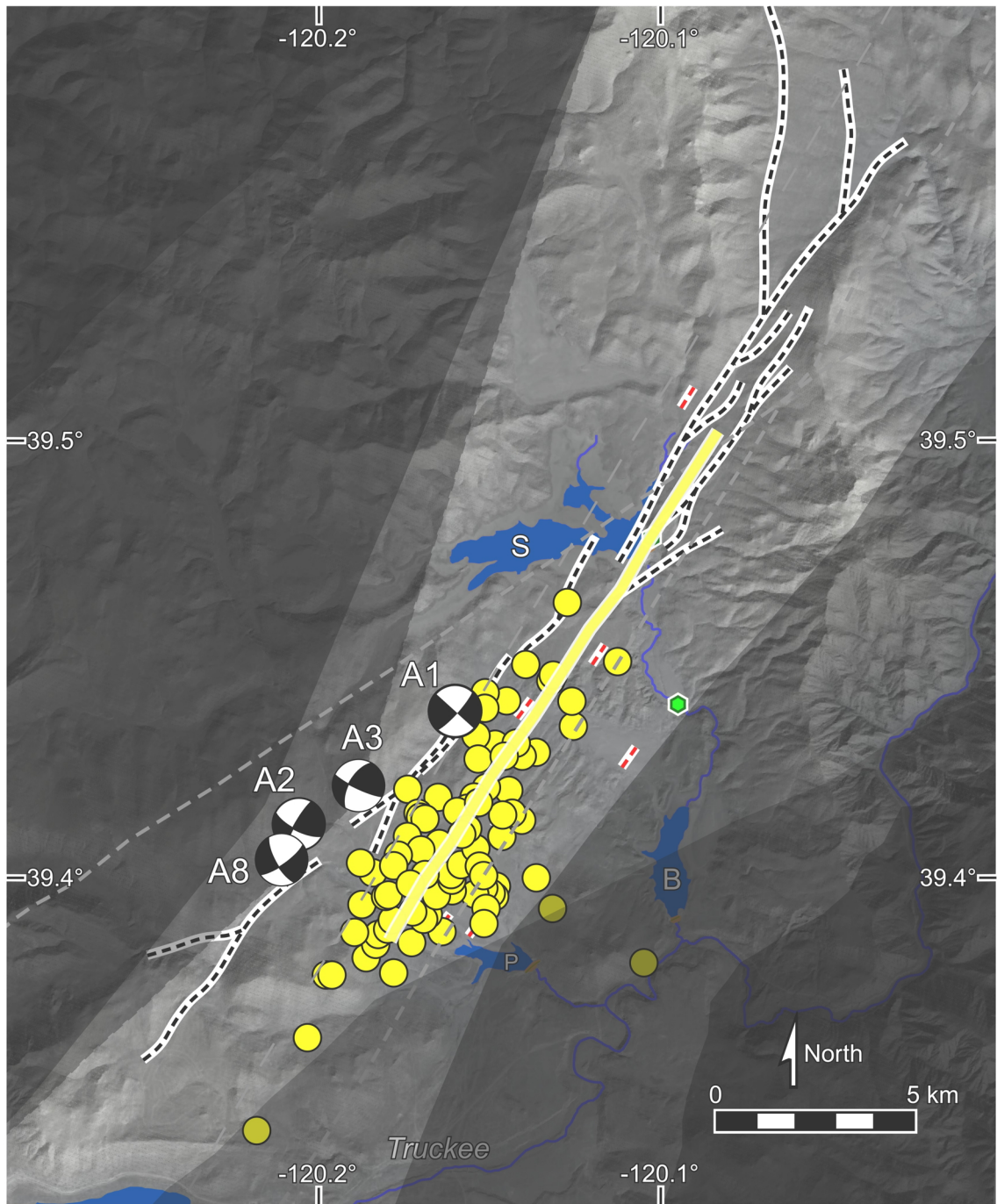Figure 14. Composite seismo-lineament map for earthquakes A1, A2, A3 and A8 (focal mechanism A). Inferred location of the Dog Valley fault is marked by dashed black curves. Red dashed lines mark places where "broken ground" was observed after the Truckee earthquake (Kachadoorian and others, 1967), whose epicenter is marked by the star. Yellow curve is the geomorphic lineament investigated in this research.

Geomorphic Analysis

The inferred location of the Dog Valley fault is based largely on the interpretation of geomorphic lineaments in the epicentral area (Hawkins and others, 1986; Grose, 2000; Olig and others, 2005). The geomorphic lineament that I selected for field investigation extends from the northwest inlet of Prosser Creek Reservoir toward the northeast abutment of Stampede Dam, intersecting Russell Valley approximately at its midpoint. This subtle lineament has an orientation of ~32° NE, placing it south of, and along a slightly smaller bearing than, the currently inferred trace of the Dog Valley fault.

Field Observations

The primary objective of the fieldwork conducted for this investigation was to locate exposed faults within the seismo-lineament swath and to identify any geomorphic features along the lineament that might be related to faulting. Field observations were restricted to locations along the lineament that could be accessed by road, the exception being observations made along the drought exposed upper shore face of the northeast abutment of the Stampede Dam. The lineament that we chose to assess was oriented ~32°, extending from the northwest inlet of Prosser Creek Reservoir to the northeast abutment of the Stampede Dam. Observations made along the lineament will be described in a NE to SW direction along the lineament, beginning with those made along the NE abutment of Stampede Dam.

Stampede Dam Northeast Abutment

The first field observations were made at a south-facing roadcut along Dog Valley Road at the northeast abutment of the Stampede Dam (figs. 15-21). Nine faults were identified in the roadcut, with several showing obvious displacement. The roadcut was composed of a Miocene-Pliocene andesitic mudflow breccia containing large angular clasts up to a meter in diameter (Birkeland, 1963; Saucedo and Wagner, 1992; Saucedo, 2005). Several of the faults exhibited a change in color across the fault surface, with the footwall comprised of an overall lighter material than the hanging wall (fig. 17). Faults 1-5, along the east side of the roadcut, had cores that ranged from a few millimeters to ~12 centimeters in width (fig. 18), comprised of a moist, dark, rusty colored gouge that was infiltrated by small root networks. Due to the coarse, poorly consolidated nature of the surrounding breccia, no shear striae were observed in any of the road cut faults.
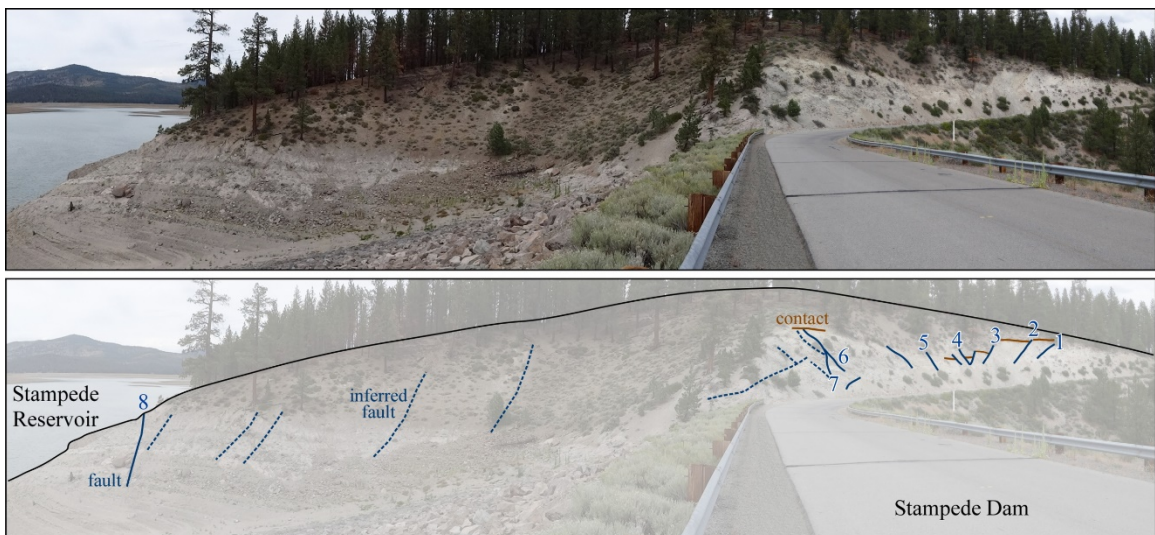

Figure 15. Panoramic overview of the faults present in the northeast abutment of the Stampede Dam. Faults to the left (west) of the road were located below the high water line of Stampede Reservoir. The road in the photograph is Dog Valley Road. Fault numbers correlate with table 5.

Figure 16. Aerial map view of the faults present in the northeast abutment of the Stampede Dam. The strike-and-dip symbols on the upper right corner of the image are faults 1-5, as labeled in figure 14 above. Orientation data for fault 8 is shown on the left (west) side of the image, and faults 9-11 are in that same area. The road in the image is Dog Valley Road. Image was taken 16 April 2015 and was acquired from Google Earth.

Table 5. Fault location and orientation data, NE abutment of Stampede Dam.

Fault No.	Latitude °N	Longitude °W	Number of Measurements	RHR Strike	Dip Angle	α_{95} Uncert	Comments
1	39.47720°	120.10222°	7	195°	36°	6°	normal separation down to the W
2	39.47721°	120.10233°	11	216°	56°	7°	normal separation down to the W
3	39.47720°	120.10249°	7	216°	50°	5°	normal separation down to the W
4	39.47719°	120.10258°	7	19°	58°	4°	normal separation down to the E
5	39.47717°	120.10271°	3	25°	77°	8°	normal separation down to the E
6	39.47715°	120.10297°	--	--	--	--	~86 cm normal sep
7	39.47715°	120.10297°	--	--	~65-72°	--	~107 cm normal sep down to the W
8	39.47684°	120.10461°	7	306°	82°	4°	across shoreface
9	--	--	7	42°	87°	1°	near #8
10	39.4769°	120.1047°	7	24°	74°	4°	near #8
11	39.4766°	120.1048°	3	186°	69°	3°	near #8

Mean orientations computed using Fisher statistics (Cronin, 2008).

Figure 17. Prominent faults located in the eastern half of the roadcut along Dog Valley Road at the northeast abutment of the Stampede Dam. Fault numbers correlate with table 5 and figure 14.

Figure 18. Photograph showing an excavated fault surface located along fault 2 exposed in the road cut along Dog Valley Road. Fault gouge zone is ~10 cm wide.

The width of the gouge zone was not consistent across all faults. Faults 6 and 7 had essentially no gouge zones that I observed. In contrast, fault 5 has a wide enough fault core to excavate and directly record strike and dip measurements with a Brunton compass. Most of the faults had no obvious markers that could be used to measure separation or slip, but faults 6 had an outcrop-parallel separation of ~86 cm and fault 7 had an outcrop-parallel separation of ~107 cm (fig. 19). The faults observed in this roadcut had strikes with an average orientation of $28^{\circ} \pm 10^{\circ}$ with dip angles between 36-56° NW and 74-87°SE.
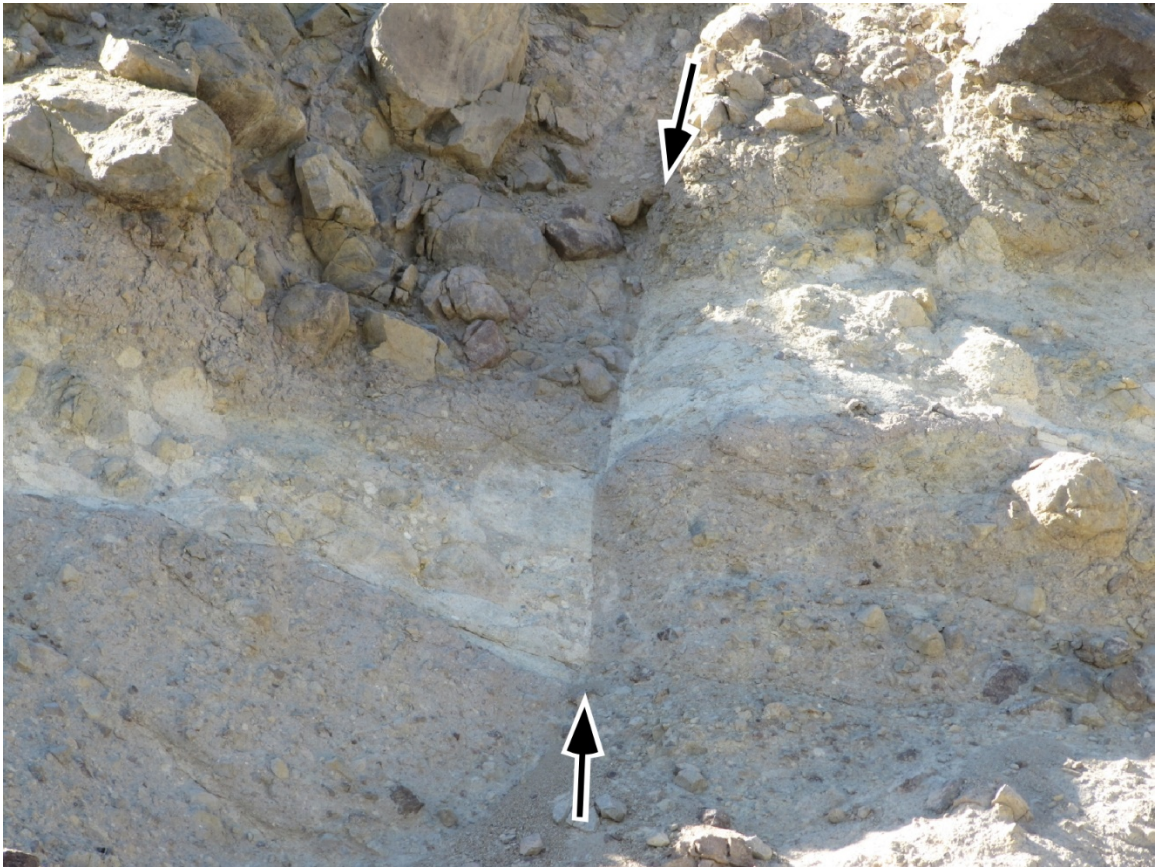

Figure 19. Photograph of separation along fault 7 exposed in the road cut along Dog Valley Road on the northeast abutment of Stampede Dam. The light colored volcanic bed is displaced ~107 cm.

Another set of faults was observed along the exposed shoreface of the northeast abutment of the Stampede Dam (fig. 20). This shoreface has been exposed as a result of the severe drought conditions that had persisted for more than a year prior to the field season. Observations made from Dog Valley Road suggested that there were several faults present in the hillslope that would otherwise be concealed by normal reservoir levels. The most obvious of these faults was fault 8, which had a split red boulder along

Figure 20. Photograph of fault 8 and related fractures taken from the Stampede Valley Dam looking north. Red curve is fault 8, yellow-black dashed curves are other joints or small faults. The location of the small split boulder used to obtain fault orientation data is shown.

the fault plane. Measurements were made along this fault in four different locations: three excavation sites along the southeast facing slope, and along the flat face of a small split boulder located at the crest of the slope. This fault has a mean orientation of 306°, 82°±4°.

The area examined directly above the water level at the time of fieldwork was heavily fractured. Some of these fractures displayed small displacements, evinced by offset clasts within the matrix material that were split along the fracture plane.

Figure 21. Photograph of the excavated fault core of fault 8. Fault core is ~15cm wide. Fault orientation data were obtained from both the excavated surface of the fault (left of center) and the face of a small split boulder (right of center).

Observations Made Along Lineament

The geomorphic lineament I chose to focus on was investigated in a northeast to southwest direction, starting along Dog Valley Road at the Stampede Dam, and ending along Prosser Dam Road at Prosser Creek Reservoir. The first feature of interest identified along the trend was a set of drainage channels parallel to the lineament that intersected Russell Valley (site b, fig. 22). The northeast reach of this drainage system paralleled Greenlee Road and continued in line with the identified lineament. The southwest reach of the drainage system was visible directly across from the northeast

reach from Russell Valley Road. The orientation of the two channels was recorded with

a Brunton compass, and found to be consistent with the orientation of the lineament. No

physical evidence of exposed faults was observed at these locations, likely due to the

presence of thick soil and glacial sediments and heavily wooded nature of the area.
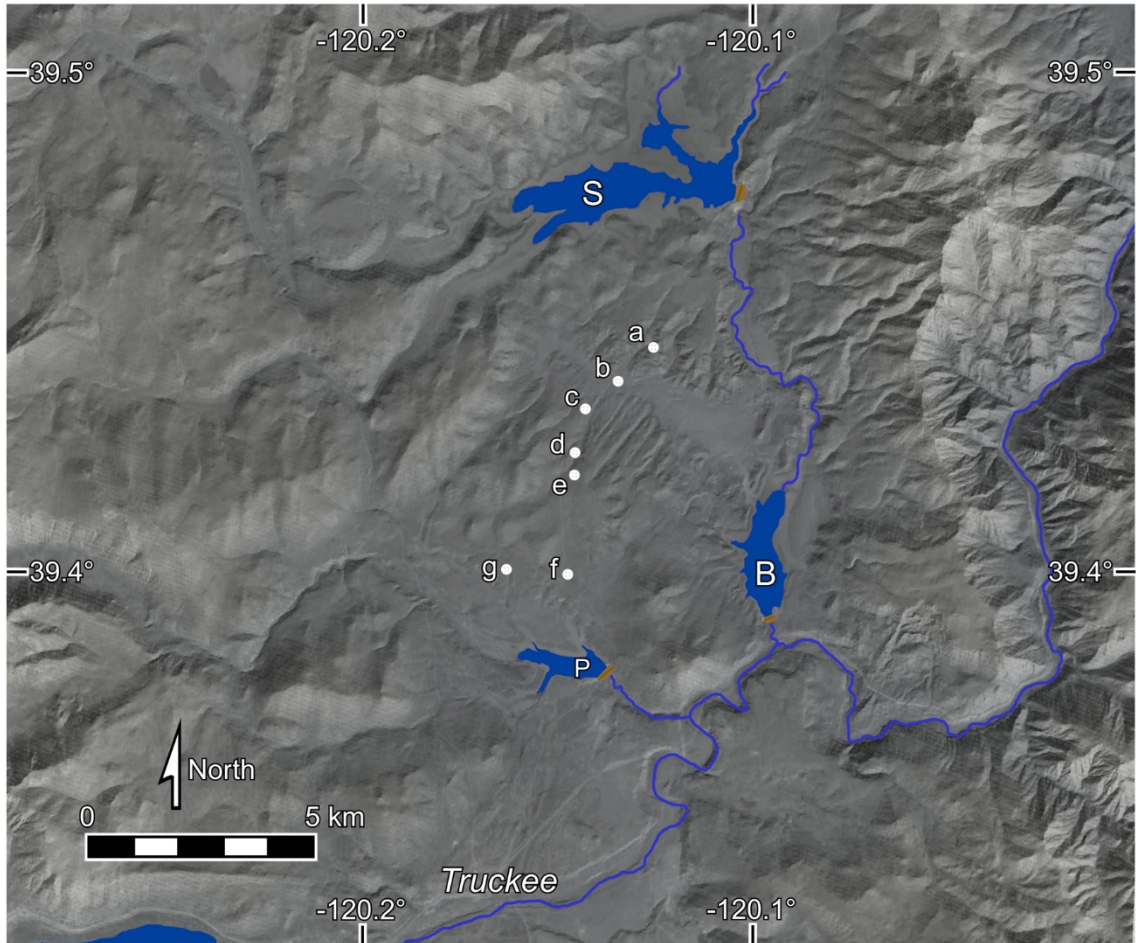

Figure 22. Locations along or adjacent to the geomorphic lineament where field observations were made.
All locations are accessible by a conventional automobile.

Figure 23. Photographs taken from site b on Russell Valley Road. Photograph A is looking northeast up the lineament along Greenlee Road. Photograph B is looking southwest along the seismo-lineament.

Moving southwest from Russell Valley, the lineament was intersected again by Dog Valley Road (site c, fig. 22). At this location, a small seasonal channel, which drained into the larger channel observed from Russell Valley Road, was observed to be in rough orientation with the lineament. Like the previous location, no physical evidence of exposed faults was observed.

Near the northern inlet of Prosser Creek Reservoir, the lineament intersected Old Reno Road. Subtle drainage features were observed on each side of the road. The northeast trending channel drained into a small meadow that was oriented at ~280° NW, and the southwest trending channel drained into the Prosser Creek Reservoir watershed. The orientation of these drainage features was later assessed in *ArcMap* and *Google Earth Pro* and found to be ~38° NE.

Figure 24. Photographs looking up and down the lineament from its intersection with Dog Valley Road at site c. Picture A is looking northeast along the lineament. Picture B is looking southwest along the lineament.

Other Observations

While exposed faults were only present along the lineament at one location, another exposed fault was observed within the general area. Approximately four kilometers south of the Stampede Dam, a fault is visible in an outcrop on a small cliff face southwest of the Little Truckee River (more southerly green hexagon in fig. 9). This fault was previously examined by Kachadoorian and others (1967) and Lindsay (2011). It did not have any obvious displacement during the 1966 M 6.0 earthquake and was not located along the lineament I investigated, so I make note of it here merely as a candidate for investigation in future studies.

Figure 2. Fault observed along the Little Truckee River approximately 5 kilometers southwest of the Stampede Dam. This fault did not fall within the seismo-lineament assessed for this field data, but is consistent with ground surface ruptures observed following the 1966 M 6.0 earthquake. Photographed by Ryan Lindsay *circa* 2010.

CHAPTER FOUR

Conclusions

The purpose of this thesis was to investigate a geomorphic lineament identified through SLAM analysis of earthquakes with epicenters located in the Truckee, California area. Using the latest version of the Seismo-Lineament Analysis Method code, twelve earthquakes that had been previously analyzed by Reed (2013) were re-assessed. Three of these earthquakes (events A2, A3 and A8; table 2) have seismo-lineaments that overlapped each other. The seismo-lineaments for these three earthquakes were then combined into a composite seismo-lineament, which was used to identify a pronounced geomorphic lineament that was isolated between the two nodal plane surface traces of the two earthquake's focal mechanisms. This geomorphic lineament aligned with the long-axis of the cloud of aftershocks that followed the 1966 Truckee earthquake, although it diverged from the inferred trend of the Dog Valley fault zone.

Evidence collected in the field suggested that faulting might have occurred along the geomorphic lineament. The geomorphic indicators of faulting that were used to delineate the potential fault trace, such as linear drainage channels and elongate meadows, were observed and documented in the study area and found to be aligned with the orientation of the composite seismo-lineament. In addition, faults observed in an outcrop located at the northeast abutment of the Stampede Dam had strikes consistent with the ~32° NE orientation of the geomorphic lineament.

The work conducted in this preliminary study generated questions that might be addressed by a more comprehensive investigation. Further investigation of the study area should be tailored to assess a wider geographic range with the goal of evaluating the

entirety of the field area, assessing any other geomorphic lineaments identified. The use

of high-resolution LiDAR data to identify such lineaments would be an invaluable asset

to a future researcher, and should be of the highest priority. A modest trench study or

geophysical survey along the geomorphic lineament identified in this study would be of

benefit, allowing a successive researcher to see beneath the thick sediments that obscured

any surface traces of a fault that may be present. Additional investigation of the

Stampede Dam abutment, spillway area, and Stampede Reservoir shore face should be

performed to both further document faults assessed in this thesis and to locate additional

faults that may be exposed in areas that were not investigated in this study. Of particular

concern is a small swale present above the high-water line of Stampede Reservoir at the

northeast abutment of Stampede Dam characterized by an abrupt lateral change in color,

which was not noticed until photographs were assessed after the completion of field

work.

REFERENCES CITED

Ashburn, J.A., Cronin, V.S., and Sverdrup, K.A., 2014, In search of the surface trace of the Dog Valley Fault near Truckee, California: Geological Society of America, Abstracts with Programs, v. 46, no. 6, p. 766; accessible online via https://gsa.confex.com/gsa/2014AM/webprogram/Paper248200.html

Birkeland, P.W., 1963, Pleistocene volcanism and deformation of the Truckee area, north of Lake Tahoe, California: Geological Society of America Bulletin, v. 74, p. 1453-1464.

Blewitt, G., Hammond, W.C., and Kreemer, C., 2009, Geodetic constraints on contemporary deformation in the northern Walker Lane – 1 Semi-permanent GPS strategy, *in* Oldow, J.S., and Cashman, P., [editors], Late Cenozoic structure and evolution of the Great Basin-Sierra Nevada transition: Geological Society of America, Special Paper 447, p. 1-15.

Bonilla, M.G., 1982, Evaluation of potential surface faulting and other tectonic deformation: U.S. Geological Survey Open-File Report 82-732, p. 58.

Burbank, D.W. and Anderson, R.S., 2001, Tectonic Geomorphology: Blackwell Science, Oxford, p. 274.

Carter, B.H., 1966, Mapping and geological investigations of Prosser Creek Dam, Boca Dam, Stampede damsite, and limited regional observations after the September 12, 1966 earthquake – Washoe Project, California-Nevada: U.S. Bureau of Reclamation Memorandum, central files, Sacramento, 10 p. Map 320-208-70 (unpublished).

Cronin, V.S., 2008, Finding the mean and 95% confidence interval of a set of strike-and-dip or lineation data: Environmental and Engineering Geoscience, v. 14, no. 2, p. 113-119.

Cronin, V.S., 2010, A draft primer on focal mechanism solutions for geologists: Teaching Quantitative Skills in the Geosciences, http://serc.carleton.edu/files/ NAGTWorkshops/structure04/Focal_mechanism_primer.pdf

Cronin, V.S., 2014a, *SLAMCode.nb* -- Projecting the nodal planes from a focal mechanism solution onto a digital elevation model surface: *Mathematica* notebook file available via http://CroninProjects.org/Vince/SLAM/SLAMcode.nb.

Cronin, V.S., 2014b, *FisherStatsSD.nb*: *Mathematica* notebook file available via http://CroninProjects.org/Vince/Codes/FisherStatsSD.nb.

Cronin, V.S., 2014c, Seismo-Lineament Analysis Method (SLAM), using earthquake focal mechanisms to help recognize seismogenic faults, *in* Grutzner, C., Choi, J-H., Edwards, P., and Kim, Y-.S., [editors], Proceeding of the 5th International INQUA Meeting on Paleoseismology, Active Tectonics and Archeoseismology, 21-27

September 2014, p. 28-31, ISBN 9791195344109 93450; available via http://CroninProjects.org/Vince/SLAM/CroninINQUA_PATA14.pdf

Cronin, V.S., and Cronin, K.E., 2014, Revised geometry of nodal-plane uncertainty volume used in the seismo-lineament analysis method to locate seismogenic faults [abs.]: Seismological Society of America Annual Meeting, Anchorage, Alaska, accessible via http://www.seismosoc.org/meetings/2014/app/index.html#_14-698

Cronin, V.S., Millard, M.A., Seidman, L.E., and Bayliss, B.G., 2008, The Seismo-Lineament Analysis Method [SLAM] – A reconnaissance tool to help find seismogenic faults: Environmental and Engineering Geoscience, v. 14, no. 3, p. 199-219.

Cronin, V.S., Schurter, G., and Sverdrup, K.A., 1993, Preliminary Landsat lineament analysis of the northern Nanga Parbat-Haramosh Massif, northwest Himalaya: Geological Society of London Special Publication, No. 74, p. 193-206.

Fisher, R.A., 1953, Dispersion on a sphere: Proceedings Royal Society, London, v. A217, no. 1130. p. 295-305.

Greensfelder, R., 1968, Aftershocks of the Truckee, California, earthquake of September 12, 1966: Bulletin of the Seismological Society of America, v. 58, no. 5, p. 1607-1620.

Grose, T.L.T., 2000, Geologic map of the Loyalton 15' quadrangle, Lassen and Plumas counties, California: California Division of Mines and Geology Open-File Report OFR 00-25, map scale 1:62,500.

Hammond, W.C., and Thatcher, W., 2007, Crustal deformation across the Sierra Nevada, northern Walker Lane, Basin and Range transition, western United States measured with GPS, 2000-2004: Journal of Geophysical Research, v. 112, B05411, doi:10.1029/2006JB004625.

Hammond, W.C., Kreemer, C., and Blewitt, G., 2009, Geodetic constraints on contemporary deformation in the northern Walker Lane – 3 Central Nevada seismic belt postseismic relaxation, *in* Oldow, J.S., and Cashman, P., [editors], Late Cenozoic structure and evolution of the Great Basin-Sierra Nevada transition: Geological Society of America, Special Paper 447, p. 33-54.

Hammond, W.C., Blewitt, G., and Kreemer, C., 2011, Block modeling of crustal deformation of the northern Walker Lane and Basin and Range from GPS velocities: Journal of Geophysical Research, v. 116, B04402, doi:10.1029/2010JB007817.

Hawkins, F.F., LaForge, R. and Hansen, R.A., 1986, Seismotectonic study of the Truckee/Lake Tahoe area northeastern Sierra Nevada, California for Stampede, Prosser Creek, Boca, and Lake Tahoe dams: U.S. Bureau of Reclamation Seismotectonic Report No. 85-4, 210 p., plate l, scale 1:250,000.

Hunter, L.E., Howle, J.F., Rose, R.S., and Bawden, G.W., 2011, LiDAR-assisted identification of an active fault near Truckee, California: Bulletin of the Seismological Society of America, v. 101, no. 3, p., 1162-1181, doi:10.1785/0120090261.

Hunter, L.E., Rose, R.S., Hilton, B.R., McCormick, W., and Crampton, T., 2010, Use of hi-resolution LiDAR in discovering the Polaris fault, Martis Creek Dam, Truckee, California, in Collaborative management of integrated watersheds: Proceedings, 30th Annual United States Society on Dams Conference, Sacramento, California, p. 281-294, available online via http://ussdams.com/proceedings/USSDproceedings2010.pdf.

Jordan, T.H., and Sverdrup, K.A., 1981, Teleseismic location techniques and their application to earthquake clusters in the south-central Pacific: Bulletin of the Seismological Society of America, v. 71, p. 1105-1130.

Jost, M.L., and Herrmann, R.B., 1989, A student's guide to and review of moment tensors: Seismology Research Letters, v. 60, p. 37-57.

Kachadoorian, R., Yerkes, R.F., and Waananen, A.O., 1967, Effects of the Truckee, California, earthquake of September 12, 1966: U.S., Geological Survey, Circular 573, p. 14.

Kreemer, C., Blewitt, G., and Hammond, W.C., 2009, Geodetic constraints on contemporary deformation in the northern Walker Lane -- 2 Velocity and strain rate tensor analysis, in Oldow, J.S., and P.H. Cashman, [editors], Late Cenozoic Structure and Evolution of the Great Basin – Sierra Nevada Transition: Geological Society of America, Special Paper 447, p. 17-31.

Lindsay, R., 2011, Seismo-lineament analysis of selected earthquakes in the Tahoe-Truckee Area, California and Nevada: Waco, Texas, Baylor University Geology Department, M.S. thesis, 147 p.

McCalpin, J., ed., 2009, Paleoseismology [2nd edition]: Amsterdam, Academic Press, 613 p.

Miller, V.C., 1961, Photogeology: McGraw-Hill, New York, 248 p.

NCEDC, 2013, accessed 2012-2013, Northern California Earthquake Data Center earthquake catalog search page, available online via quake.geo.berkeley.edu/ncedc/catalog-search.html.

Olig, S., Sawyer, T., Wright, D., Terra, F., and Anderson, L., 2005, Preliminary seismic source characterization of faults near Stampede and Prosser Creek dams - Washoe project and Boca Dam - Truckee storage project, U.S. Department of the Interior, Bureau of Reclamation, Denver, 65 p.

Putirka, K.D., and Busby, C.J., 2011, Introduction: Origin and evolution of the Sierra

Nevada and Walker Lane, *Geosphere*, v. 7, no. 6, p. 1269-1272

Ray, R.G., 1960, Aerial photographs in geologic interpretation and mapping: U.S. Geological Survey Professional Paper 373, p. 230.

Reasenberg, P.A., and Oppenheimer, D., 1985, FPFIT, FPPLOT, and FPPAGE: Fortran computer programs for calculating and displaying earthquake fault-plane solutions: U.S. Geological Survey, Open-File Report, no. 85-739.

Reed, T.H., 2013, Spatial correlation of earthquakes with two known and two suspected seismogenic faults, north Tahoe-Truckee area, California: M.S. thesis, Baylor University, Waco, Texas, 96 p.

Ryall, A., Van Wormer, J.D., and Jones, A.J., 1968, Triggering of micro-earthquakes by earth tides, and other features of the Truckee, California, earthquake sequence of September, 1966: Bulletin of the Seismological Society of America, v. 58, no. 1, p. 215-248.

Saucedo, G.J., compiler, 2005, Geologic map of the Lake Tahoe Basin, California and Nevada, scale 1:100,000: California Geological Survey, Regional Geological Map Series, Map No. 4, accessible online via http://www.quake.ca.gov/gmaps/RGM/tahoe/tahoe.html

Saucedo, G.J., and Wagner, D.L., 1992, Geologic map of the Chico quadrangle, scale 1:250,000, California Division of Mines and Geology, regional geologic map 7A, available online via http://ngmdb.usgs.gov/Prodesc/proddesc_63087.htm

Schaff, D.P. and Waldhauser, F., 2005, Waveform cross-correlation-based differential travel-time measurements at the Northern California Seismic Network, Bulletin of the Seismological Society of America, v. 95, p. 2446-2461.

Scherbaum, F., Kuehn, N., and Zimmermann, B., 2009, Earthquake focal mechanism: Wolfram Demonstration Project, accessed June 6, 2013 via http://demonstrations.wolfram.com/EarthquakeFocalMechanism/

Stewart, J.H., 1988, Tectonics of the Walker Lane belt western Great Basin – Mesozoic and Cenozoic deformation in a shear zone. In: Ernst, W.G. (Ed.), Metamorphism and Crustal Evolution of the Western United States. Englewood Cliffs, Prentice Hall, New Jersey, pp. 683-713.

Tsai, Y-B., and Aki, K., 1970, Source mechanism of the Truckee, California earthquake of September 12, 1966: Bulletin of the Seismological Society of America. v. 60, no. 4, p. 1199-1208.

USACE, 2012, Martis Creek dam safety modification study: U.S. Army Corps of Engineers, accessed 10 March 2015 via http://www.spk.usace.army.mil/Missions/CivilWorks/MartisCreekDam.aspx

USBR, 2011, Stampede dam: U.S. Bureau of Reclamation, web resource accessed on 24 April 2014 via http://www.usbr.gov/projects/

USGS, 2014, National Map Viewer: U.S. Geological Survey, available online via http://viewer.nationalmap.gov/viewer/.

USGS, 2015, Quaternary Fault and Fold Database of the United States: U.S. Geological Survey, accessed 2014-2015, available online via http://earthquake.usgs.gov/hazards/qfaults/.

Waldhauser, F., 2001, HypoDD -- A program to compute double-difference hypocenter locations: U.S. Geological Survey Open-File Report 01-113.

Waldhauser, F., 2009, Near-real-time double-difference event location using long-term seismic archives, with application to northern California: Bulletin of the Seismological Society of America, v. 99, no. 5, p. 2736-2748, doi: 10.1785/0120080294

Waldhauser, F., 2013, Real-time double-difference earthquake locations for northern California, accessed 6 August 2013 via http://ddrt.ldeo.columbia.edu.

Waldhauser, F., and Ellsworth, W.L., 2000, A double-difference earthquake location algorithm -- method and application to the northern Hayward Fault, CA: Bulletin of the Seismological Society of America, v. 90, p. 1353-1368.

Waldhauser, F. and Schaff, D.P., 2008, Large-scale relocation of two decades of Northern California seismicity using cross-correlation and double-difference methods: Journal of Geophysical Research, v. 113, B08311, doi:10.1029/2007JB005479

APPENDICES

Figure A1. Raw output of *SLAMcode.nb* for earthquake A1 on 12 September 1966. Small square marks the epicenter at latitude 39.438°N longitude 120.160°W. Nodal plane dip direction is 134°, dip angle 80°, rake 180°. Hypocenter depth was 10 km. The curves indicate the extent of the seismo-lineament. The image is aligned with the UTM grid, so the image would have to be rotated ~1.73° clockwise to be aligned with the geographic coordinate system at/near its center. North is toward the top of the page.

Figure A2. Raw output of *SLAMcode.nb* for earthquake A2 on 3 July 1983. Small square marks the epicenter at latitude 39.412°N longitude 120.206°W. Nodal plane dip direction is 300°, dip angle 80°, rake 20°. Hypocenter depth was 11.05 km. The curves indicate the extent of the seismo-lineament. The image is aligned with the UTM grid, so the image would have to be rotated ~1.73° clockwise to be aligned with the geographic coordinate system at/near its center. North is toward the top of the page.

Figure A3. Raw output of *SLAMcode.nb* for earthquake A3 on 30 August 1992. Small square marks the epicenter at latitude 39.42047°N longitude 120.18852°W. Nodal plane dip direction is 301°, dip angle 61°, rake 12°. Hypocenter depth was 5.34 km. The curves indicate the extent of the seismo-lineament. The image is aligned with the UTM grid, so the image would have to be rotated ~1.73° clockwise to be aligned with the geographic coordinate system at/near its center. North is toward the top of the page.
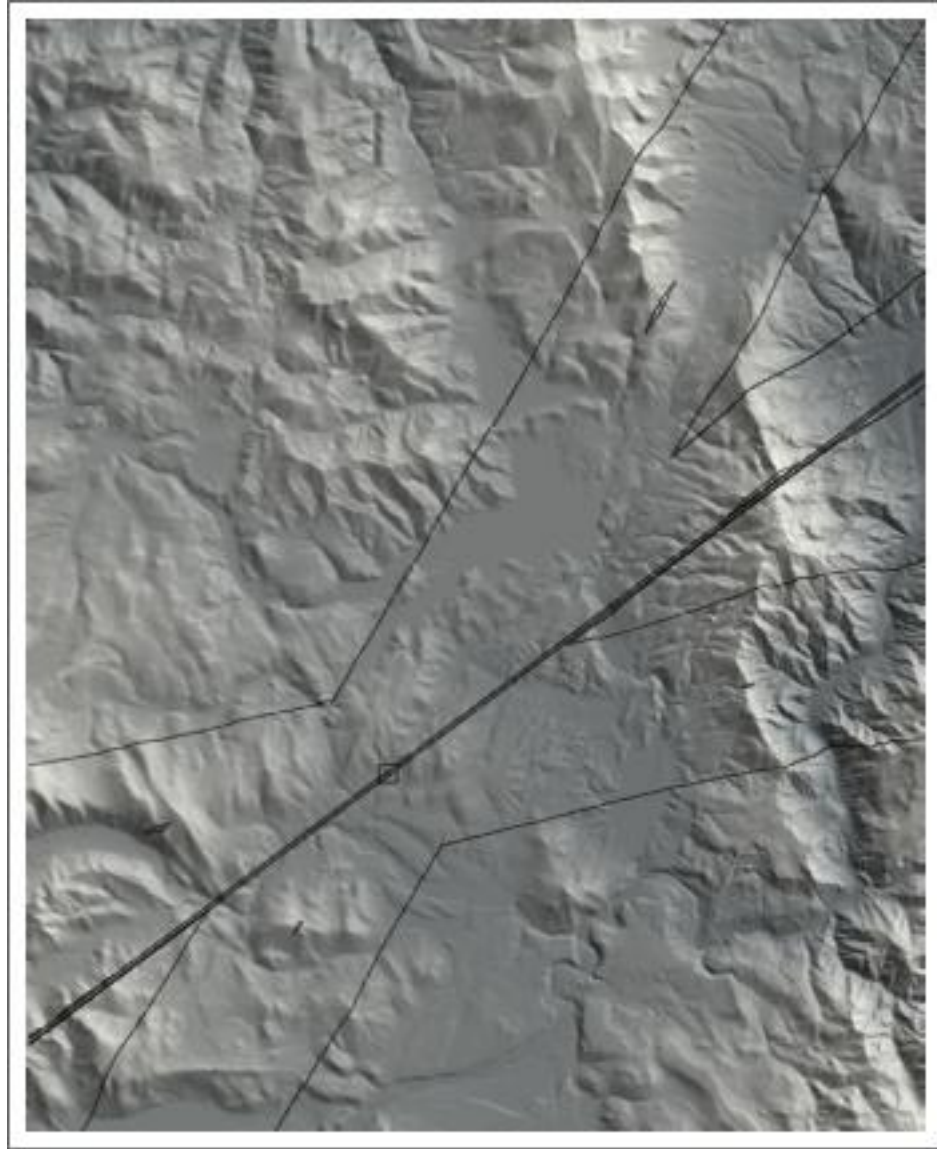
Figure A4. Raw output of *SLAMcode.nb* for earthquake A4 on 6 August 1993. Small square marks the epicenter at latitude 39.41621°N longitude 120.18018°W. Nodal plane dip direction is 333°, dip angle 48°, rake 59°. Hypocenter depth was 0.368 km. The curves indicate the extent of the seismo-lineament. The image is aligned with the UTM grid, so the image would have to be rotated ~1.73° clockwise to be aligned with the geographic coordinate system at/near its center. North is toward the top of the page.

Figure A5. Raw output of *SLAMcode.nb* for earthquake A4 on 6 August 1993. Small square marks the epicenter at latitude 39.41621°N longitude 120.18018°W. Nodal plane dip direction is 115°, dip angle 50°, rake -70°. Hypocenter depth was 0.368 km. The curves indicate the extent of the seismo-lineament. The image is aligned with the UTM grid, so the image would have to be rotated ~1.73° clockwise to be aligned with the geographic coordinate system at/near its center. North is toward the top of the page.

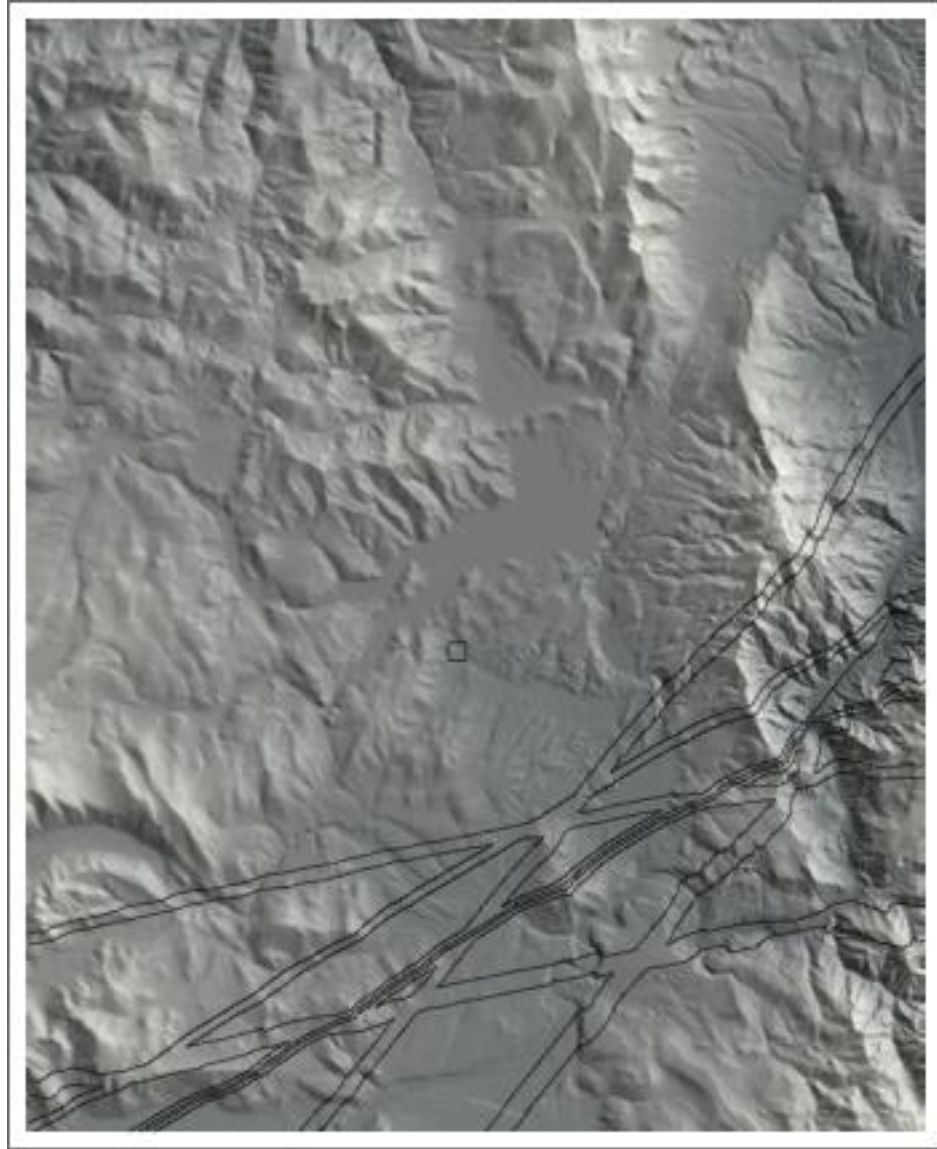Figure A6. Raw output of *SLAMcode.nb* for earthquake A4 on 6 August 1993. Small square marks the epicenter at latitude 39.41621°N longitude 120.18018°W. Nodal plane dip direction is 325°, dip angle 90°, rake 30°. Hypocenter depth was 0.368 km. The curves indicate the extent of the seismo-lineament. The image is aligned with the UTM grid, so the image would have to be rotated ~1.73° clockwise to be aligned with the geographic coordinate system at/near its center. North is toward the top of the page.
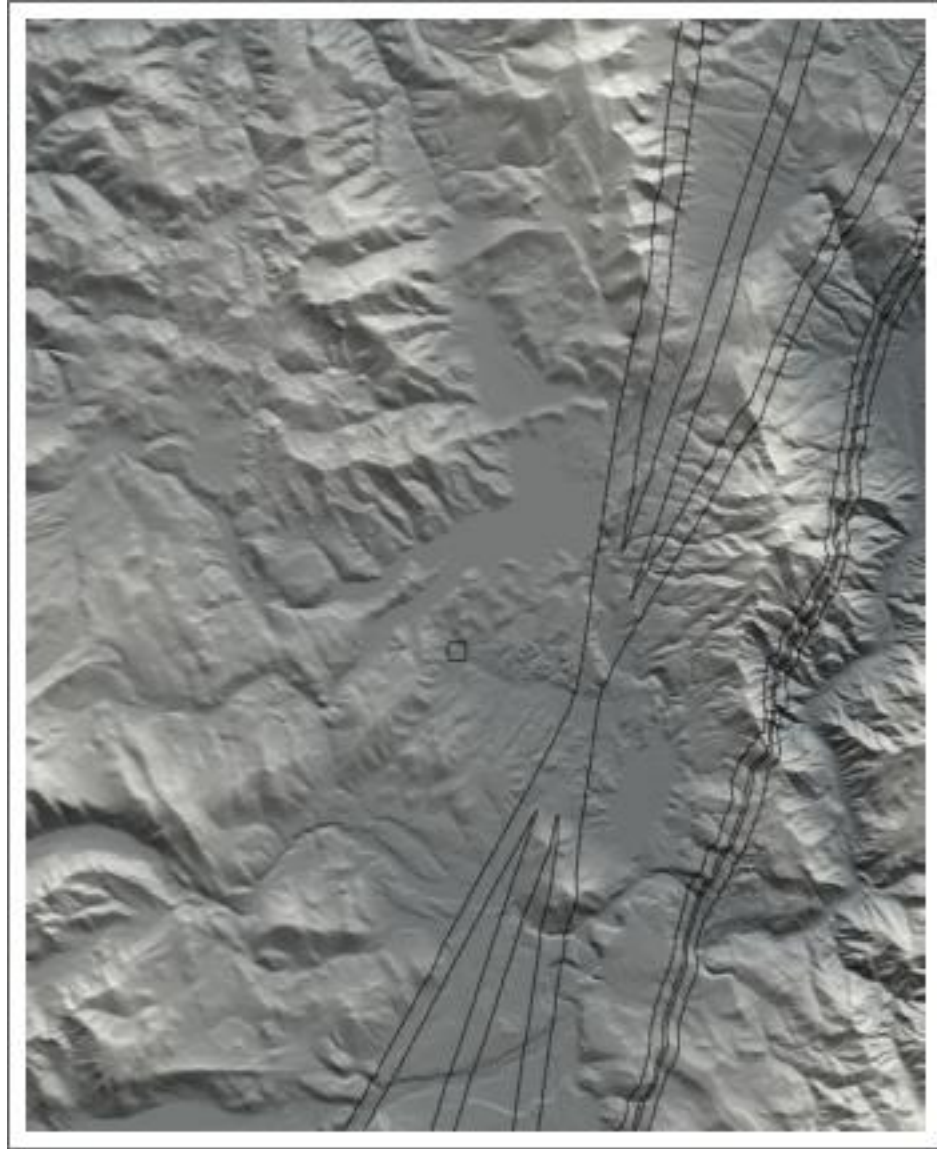
Figure A7. Raw output of *SLAMcode.nb* for earthquake A5 on 15 January 1998. Small square marks the epicenter at latitude 39.44810°N longitude 120.15511°W. Nodal plane dip direction is 331°, dip angle 41°, rake 49°. Hypocenter depth was 4.636 km. The curves indicate the extent of the seismo-lineament. The image is aligned with the UTM grid, so the image would have to be rotated ~1.73° clockwise to be aligned with the geographic coordinate system at/near its center. North is toward the top of the page.

Figure A8. Raw output of *SLAMcode.nb* for earthquake A5 on 15 January 1998. Small square marks the epicenter at latitude 39.44810°N longitude 120.15511°W. Nodal plane dip direction is 290°, dip angle 35°, rake 30°. Hypocenter depth was 4.636 km. The curves indicate the extent of the seismo-lineament. The image is aligned with the UTM grid, so the image would have to be rotated ~1.73° clockwise to be aligned with the geographic coordinate system at/near its center. North is toward the top of the page.

Figure A9. Raw output of *SLAMcode.nb* for earthquake A5 on 15 January 1998. Small square marks the epicenter at latitude 39.44810°N longitude 120.15511°W. Nodal plane dip direction is 175°, dip angle 73°, rake 121°. Hypocenter depth was 4.636 km. The curves indicate the extent of the seismo-lineament. The image is aligned with the UTM grid, so the image would have to be rotated ~1.73° clockwise to be aligned with the geographic coordinate system at/near its center. North is toward the top of the page.
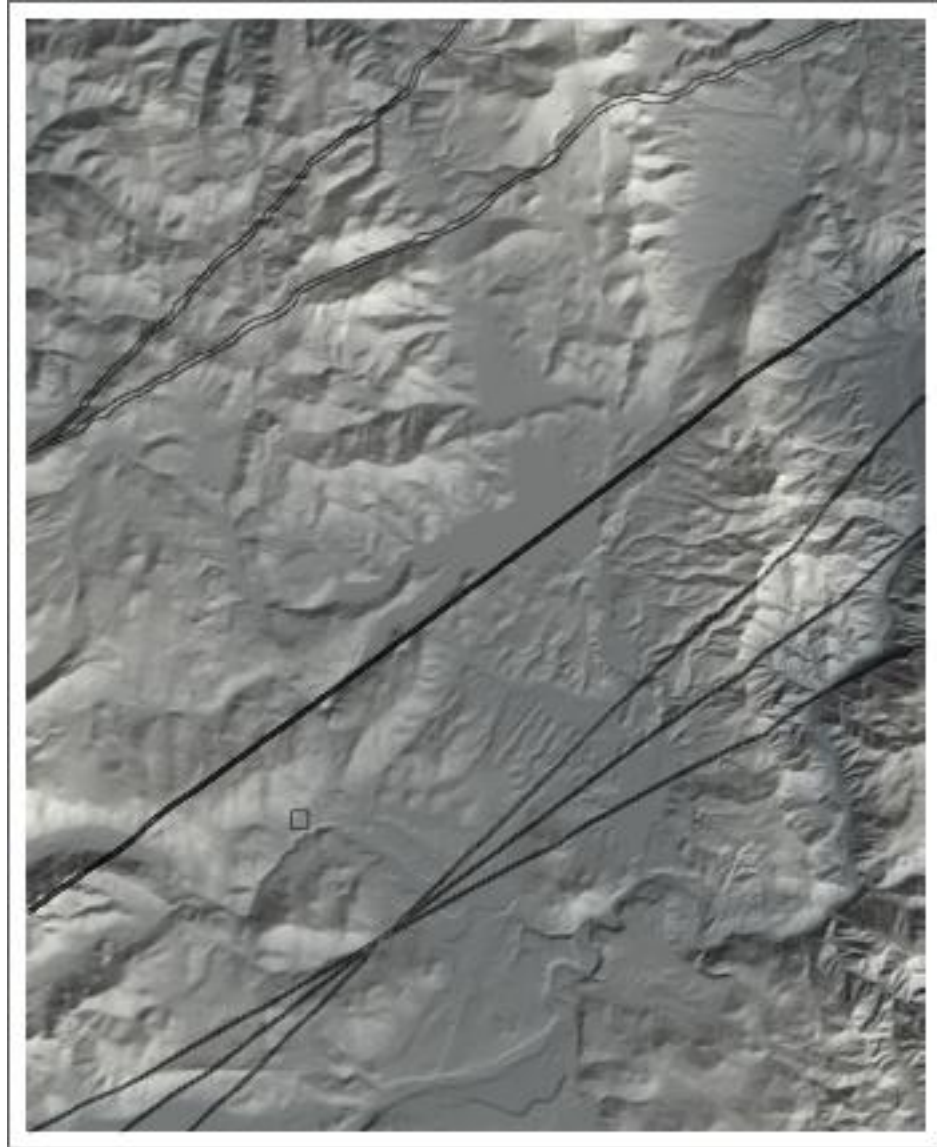
Figure A10. Raw output of *SLAMcode.nb* for earthquake A8 on 12 June 2004 at 14 hours 49 minutes. Small square marks the epicenter at latitude 39.40479°N longitude 120.21070°W. Nodal plane dip direction is 145°, dip angle 75°, rake -20°. Hypocenter depth was 7.292 km. The curves indicate the extent of the seismo-lineament. The image is aligned with the UTM grid, so the image would have to be rotated ~1.73° clockwise to be aligned with the geographic coordinate system at/near its center. North is toward the top of the page.
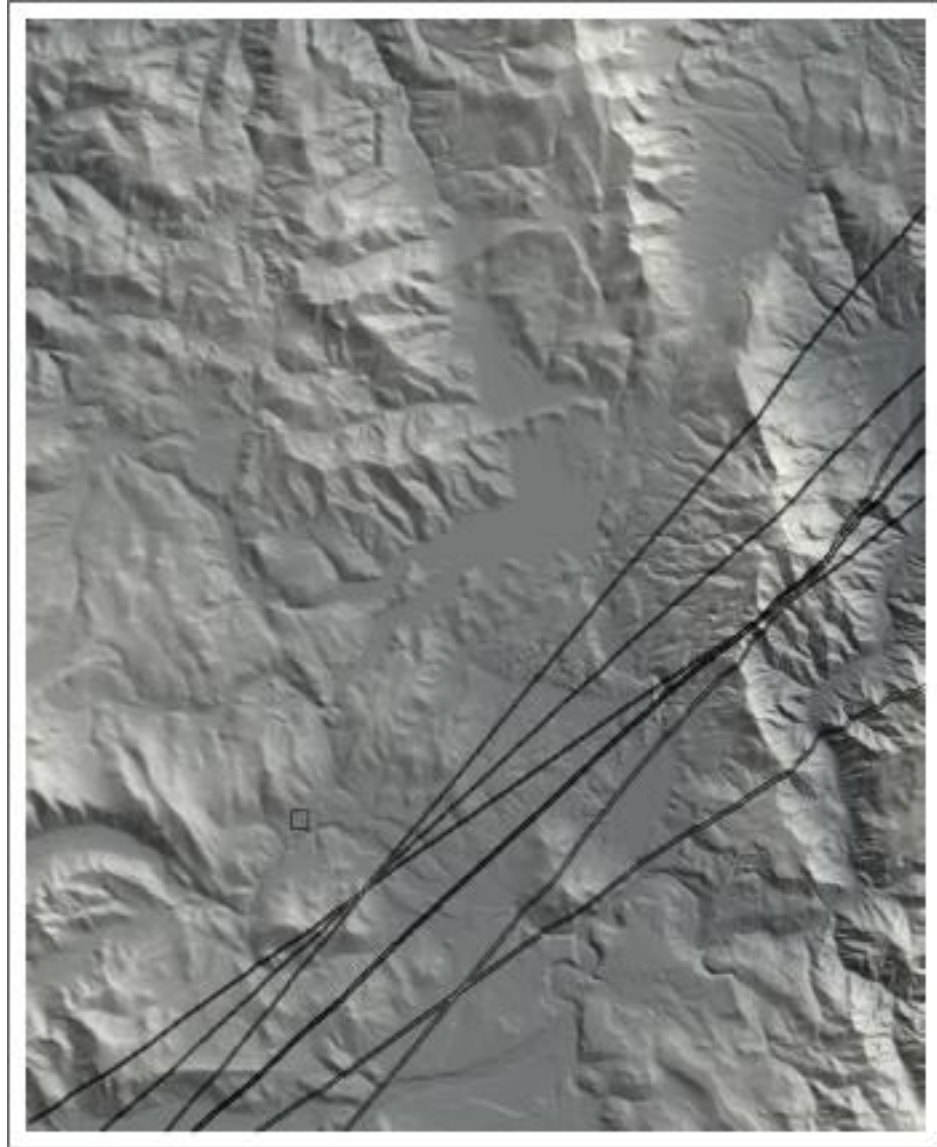
Figure A11. Raw output of *SLAMcode.nb* for earthquake A8 on 12 June 2004 at 14 hours 49 minutes. Small square marks the epicenter at latitude 39.40479°N longitude 120.21070°W. Nodal plane dip direction is 319°, dip angle 63°, rake -53°. Hypocenter depth was 7.292 km. The curves indicate the extent of the seismo-lineament. The image is aligned with the UTM grid, so the image would have to be rotated ~1.73° clockwise to be aligned with the geographic coordinate system at/near its center. North is toward the top of the page.
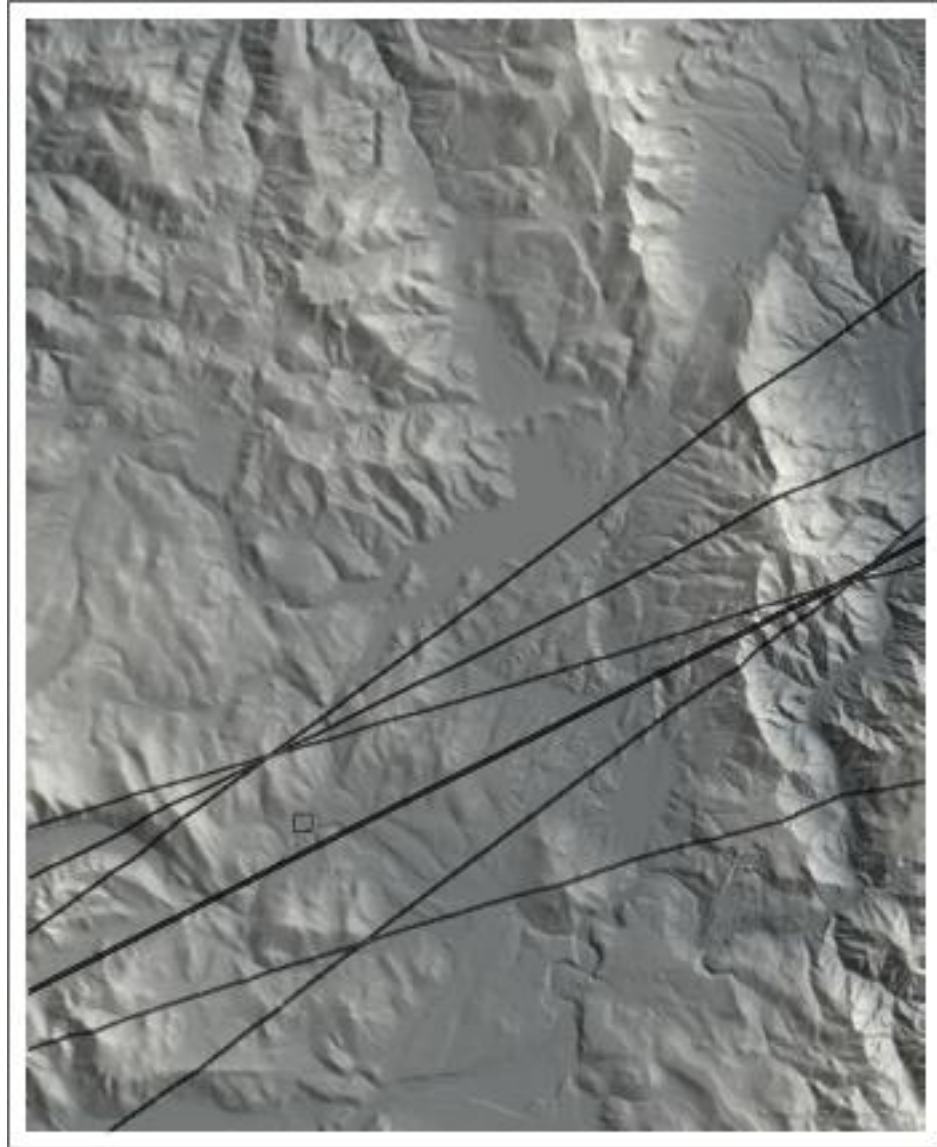
Figure A12. Raw output of *SLAMcode.nb* for earthquake A9 on 12 June 2004 at 15 hours 4 minutes. Small square marks the epicenter at latitude 39.40392°N longitude 120.20964°W. Nodal plane dip direction is 335°, dip angle 85°, rake 40°. Hypocenter depth was 7.350 km. The curves indicate the extent of the seismo-lineament. The image is aligned with the UTM grid, so the image would have to be rotated ~1.73° clockwise to be aligned with the geographic coordinate system at/near its center. North is toward the top of the page.
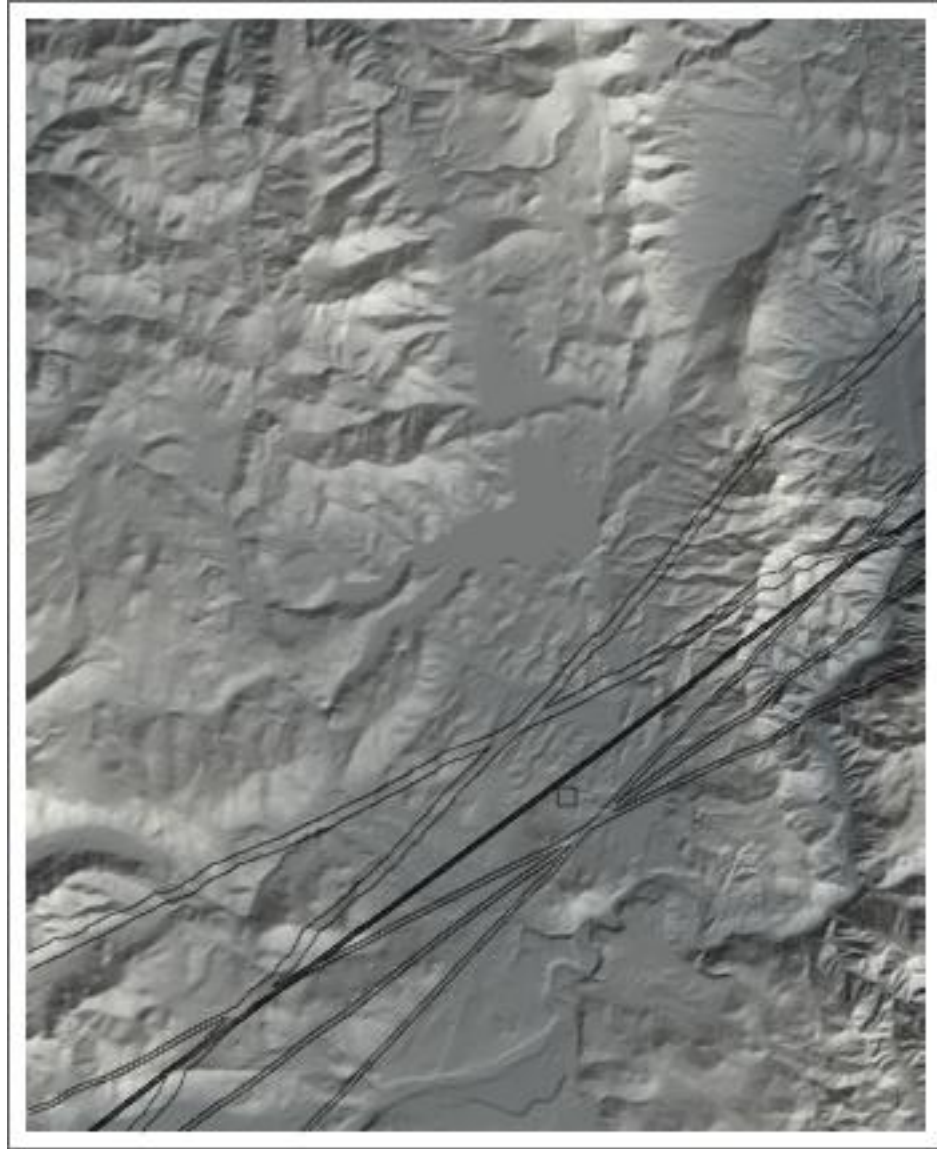
Figure A13. Raw output of *SLAMcode.nb* for earthquake A12 on 23 December 2011. Small square marks the epicenter at latitude 39.40871°N longitude 120.11916°W. Nodal plane dip direction is 145°, dip angle 80°, rake 0°. Hypocenter depth was 0.882 km. The curves indicate the extent of the seismo-lineament. The image is aligned with the UTM grid, so the image would have to be rotated ~1.73° clockwise to be aligned with the geographic coordinate system at/near its center. North is toward the top of the page.